Fundamentals of Astrodynamics and Applications

Change Summary

April 19, 2000
May 27, 2004 (pdf version)

by David Vallado

These change sets are an on-going document of errors encountered in the book. My goal is to maintain a listing of all changes for future revisions. I appreciate any questions you find in this document, or in the text.

You may reach me at work
dvallado@agi.com
or at home
valladodl@worldnet.att.net

I use the following notations for each change:
Correction -
New Information -
Clarification- of the concept
Wording - Improve structure, fix fonts, etc.
Spelling -
Changes are underlined to indicate the portion that has changed. In some cases, the underline isn't visible for words that have been deleted. I circle these occurances. Equations also do not show the specific changes.

I've made some changes throughout the text and haven't listed individual occurances.
1. I now distinguish between the FK5 system, and the J2000 epoch, thus the references to J2000 are mostly chganged to FK5.

Chapters 1, 3, 9 have been updated so the changes here reflect only corrections that were previously identified. Some topics have been moved between chapters.

Chapter 1.

pg 11 : Clarification / Correction

Figure 1-3. Geometry for Conic Sections. We create conic sections by recognizing that the sum of the distance from both foci to *any* point on the orbit is constant. The ratio of the distance from a focus to the orbit and the distance to the directrix is also a constant called the eccentricity, *e*. The closest point in the orbit to the primary focus, *F*, is the radius of periapsis, r_p. The distance *l* is a standard quantity used to describe conic sections.

moves, the length from each focus changes, and the pencil traces out the ellipse. Mathematically (Prussing and Conway, 1993, 62), for any point on the conic section,

$$\begin{aligned} r_{F'} + r_F &= \text{constant} = 2a \\ \left| r_F - r_{F'} \right| &= \text{constant} = 2c \end{aligned} \tag{1-2}$$

pg 12 : Clarification

Figure 1-4. Elliptical Orbits. An elliptical orbit has two distinct foci with the primary focus, *F*, at the center of the Earth. The radius of apoapsis, r_a, and periapsis, r_p, denote the extreme points of the ellipse. The semimajor axis, *a*, and the semiminor axis, *b*, describe the shape of the orbit. Half the distance between the foci is *c*, and the semiparameter, *p*, locates the orbit distance normal from the major axis at the focus.

This expression is useful because it relates any vertical part of an ellipse, y_e, to the corresponding part of a circle, y_c, with the semi-major axis, *a*. The following conversion finds the vertical distance on the circle, y_c, and the vertical distance for the ellipse, y_e. We'll use this scaling factor in many derivations throughout the book.

$$y_e = \frac{b}{a} y_c = y_c \sqrt{1 - e^2} \qquad y_c = \frac{y_e}{\sqrt{1 - e^2}} \tag{1-6}$$

pg 15 : Spelling

Figure 1-5. Hyperbolic Orbits. For a hyperbolic orbit, the semimajor axis is negative, and the eccentricity is larger than 1.0. Notice the rapid departure from the Earth with a *modest* eccentricity. The orbit approaches the dashed-line asymptotes. Hyperbolas occur in pairs called branches. The second branch is a mirror image of the first branch about the conjugate axis, shown as the dashed vertical line.

pg 16 : Correction to Figure

.

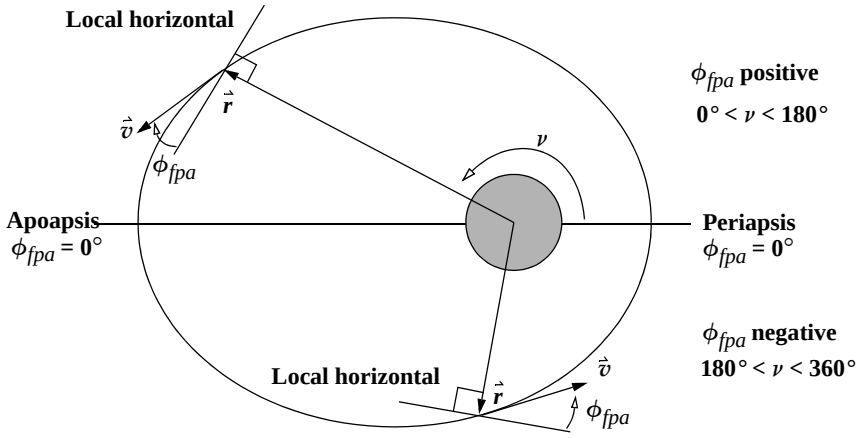

Figure 1-9. Geometry for the Flight-path Angle. The flight-path angle is always measured from the local horizontal to the velocity vector. It's always positive while the satellite travels from periapsis to apoapsis and negative for travel from apoapsis to periapsis. I've exaggerated the diagram for clarity.

pg 17 : Correction

We can define more constants to represent the Earth's exact shape, but they're usually reserved for advanced applications. I've summarized these values with many conversions in the table on the inside back cover of this book.

pg 18 : Clarification

Using Eq. (1-4) and $R_{\oplus}$ as the semimajor axis, we can also derive the *flattening* and the *eccentricity of the Earth*, $e_{\oplus}$:

pg 27 : Correction

As an aside, we can also find the reduced latitude ($\phi_{rd} = \text{TAN}^{-1}\left(\text{TAN}(\phi_{gd})\sqrt{1-e_{\oplus}^2}\right)$) and then use Eq. (1-15) to find the components directly.

pg 31 : Clarification

model (OSU-91A) is complete through degree and order 360. Models based on satellite observations are sometimes smaller. Models include the *Joint Gravity Model* (JGM-3, 70 × 70), the Defense Mapping Agency's *World Geodetic Survey* (WGS-84, 41 × 41), the *Goddard Earth Model* (GEM, 50 × 50), and others. A larger and combined model (EGM-96) came out in late 1996. Typically, accuracy requirements drive the maximum

pg 37 : Clarification

Figure 1-19. Heliocentric Coordinate System, *XYZ*. The primary direction for this system is the vernal equinox, ♈, on the first day of spring. Seasonal dates for the Northern Hemisphere are approximate due to small perturbational forces on the Earth.

pg 44 : Correction

fundamental plane, as shown in Fig. 1-26. We find the principal axis, *E*, by rotating in the equatorial plane positively from the vernal equinox along the equator to the orbit's ascending node. Next we rotate from the equator to the orbital plane through the .

pg 50 : Correction

$$\vec{r}_{site} = r[\cos(\phi_{gc})\cos(\theta_{LST})\hat{I} + \cos(\phi_{gc})\sin(\theta_{LST})\hat{J} + \sin(\phi_{gc})\hat{K}]$$
$$\hat{Z} = \frac{\vec{r}_{site}}{|\vec{r}_{site}|} \qquad \hat{E} = \frac{\hat{K}\times\hat{Z}}{|\hat{K}\times\hat{Z}|} \qquad \hat{S} = \hat{E}\times\hat{Z} \tag{1-22}$$

pg 53 : Correction

Transformations between *ECEF* and *IJK* ignoring precession, nutation, and polar motion involve only θ_{LST} [Eq. (1-42)]. EFG transformations use θ_{AST} [Eq. (1-63)].

pg 55 : Correction

$$\vec{r}_{EQW} = \text{ROT3}(-f_r\Omega)\text{ROT1}(i)\text{ROT3}(\Omega)\vec{r}_{IJK}$$
$$\vec{r}_{IJK} = \text{ROT3}(-\Omega)\text{ROT1}(-i)\text{ROT3}(f_r\Omega)\vec{r}_{EQW} \tag{1-37}$$

$$\left[\frac{EQW}{IJK}\right] = \begin{bmatrix} \cos^2(\Omega) + f_r \cos(i) \sin^2(\Omega) & \cos(\Omega)\sin(\Omega)\{1 - f_r \cos(i)\} & -f_r \sin(i) \sin(\Omega) \\ f_r \cos(\Omega)\sin(\Omega)\{1 - f_r \cos(i)\} & f_r \sin(\Omega)^2 + \cos(i)\cos^2(\Omega) & \sin(i)\cos(\Omega) \\ \sin(i)\sin(\Omega) & -\sin(i)\cos(\Omega) & \cos(i) \end{bmatrix}$$

---

pg 61 : Correction

where $\omega_\oplus$ is the Earth's mean angular rotation in degrees (or radians in the table on the inside back cover) per solar second and *UT*1 is the universal time in solar seconds. Note that units may need to be changed to be consistent with θ_{GST0}. The following algorithm for *GST* and *LST* and an example illustrate this method.

Reduce this quantity to a result within the range of 360° (–31.423 618 46°). Next, update *GST* for the current *UT*1 ($\omega_\oplus$ is from the table on the inside back cover).

---

pg 62 : Clarification

Next find *ED* = 232 from Table 1-5 (1992 is a leap year). Then, update *ED* with 12/24 + 14/1440 for *UT*.

ED = 232.509 722 222 elapsed days from January 1

---

pg 67 : Clarification

February as months 13 and 14, respectively. Thus, if *mo* = 1 or 2, then we assign *yr* = *yr* – 1 and *mo* = *mo* +12. The daily time is added as in the final term of Algorithm 2. For Julian calendar dates, set *B* = 0.

---

pg 72-73 : Correction

($yr, mo, day, UTC, \Delta UT1, \Delta AT \Rightarrow UT1, TAI, TDT, TDB, T_{UT1}, T_{TDT}, T_{TDB}$)

Daylight Savings Time exists in the Mountain Standard Time Zone. Therefore, from Table 1-4, we must add six hours to get *UTC*. We find *UT*1 as

Now find the Julian centuries of *TDT* using Eq. (1-50):

Finally, determine additional Julian centuries for specific applications. Remember to first find the Julian date for each time before determining the centuries. Using the appropriate *JD* with Eq. (1-50), (JD_{TDB} = 2,448,026.197 189 644 3; JD_{UT1} = 2,448,026.196 528 329 6)

$$T_{TDB} = \frac{JD_{TDB} - 2{,}451{,}545.0}{36{,}525} = -0.096\,339\,570\,440\,9 \quad T_{UT1} = -0.096\,339\,588\,546\,9$$

---

pg 76 : Clarification

motion of the ecliptic plane due to general precession causes the equinox to move along the equator, and we associate its orientation with an ideal inertial frame on a specific date,

pg 78 : Correction

$$T_o = \frac{JD_{start} - J2000}{36{,}525} \qquad T_\Delta = \frac{JD_{end} - JD_{start}}{36{,}525}$$

$$\begin{aligned}
\zeta &= (2306.2181'' + 1.396\,56T_o - 0.000\,139T_o^2)T_\Delta + (0.301\,88 - 0.000\,344T_o)T_\Delta^2 + 0.017\,998T_\Delta^3 \\
\Theta &= (2306.2181'' - 0.853\,30T_o - 0.000\,217\,T_o^2)T_\Delta + (-0.426\,65 - 0.000\,217T_o)T_\Delta^2 - 0.041\,833T_\Delta^3 \\
z &= (2304.310\,9'' + 1.396\,56T_o - 0.000\,139T_o^2)T_\Delta + (1.094\,68 + 0.000\,066T_o)T_\Delta^2 + 0.018\,203T_\Delta^3
\end{aligned} \tag{1-55}$$

T_{TDB} [Eq. (1-50)] represents the number of Julian centuries of *TDB* from the base epoch (J2000). The order of the rotations is important, and to complete the transformation due to precession, we have identical relations for position and velocity.

$$\begin{aligned}
\vec{r}_{ECImod} &= \text{ROT3}(-z)\text{ROT2}(\Theta)\text{ROT3}(-\zeta)\vec{r}_{J2000mod} \\
\vec{v}_{ECImod} &= \text{ROT3}(-z)\text{ROT2}(\Theta)\text{ROT3}(-\zeta)\vec{v}_{J2000mod}
\end{aligned} \tag{1-56}$$

pg 79 : Clarification

The next transformation accounts for the periodic effects contributed primarily by the Moon. The nutation is more lengthy to determine because of the complexity of the motion. We determine the primary variation from a trigonometric series of 106 terms. The result is periodic, rather than secular like the precession effect. You can also find a more accurate nutation (a 4 term series) from Seidelmann (1992, 117), and an account for the effect from the planets which is a separate 85 term series. Adding all these effects transforms the *mean* equator of date to the *true* equator of date with the primary vector pointing to the *true equinox*.

pg 81 : Clarification

mean and true equinoxes onto the true equator—thus a simple formula for the *equation of the equinoxes* is $\Delta\Psi\text{COS}(\epsilon)$, which we saw in the approximate form of the nutation matrix. We use the equation of the equinoxes to convert between apparent and mean sidereal times. We can easily derive this relation from the right triangle having a central angle ϵ. Be aware that before January 1, 1997, the last two terms, $+0.002\,64''\ \text{SIN}(\Omega_{\leftmoon}) + 0.000\,063\ \text{SIN}(2\Omega_{\leftmoon})$, were not used. From Fig. 1-34, we find the Greenwich apparent sidereal time, θ_{AST}, using the Greenwich mean sidereal time [Eq. (1-51) and Eq. (1-45)], plus the equation of the equinoxes:

$$\begin{aligned}
EQ_{equinox} &= \Delta\Psi\,\text{COS}(\epsilon) + 0.002\,64''\,\text{SIN}(\Omega_{\leftmoon}) + 0.000\,063\,\text{SIN}(2\Omega_{\leftmoon}) \\
\theta_{AST} &= \theta_{GST} + EQ_{equinox}
\end{aligned} \tag{1-63}$$

pg 82 : Clarification

A final transformation accounts for the North Pole's changing location. Seidelmann (1982) defines polar motion as the "movement of the rotation axis with respect to the crust of the Earth". The coefficients are measured by the ***International Polar Motion Service*** (IPMS) and published by ***International Earth Rotation Service*** (IERS, formerly the *Bureau International de l'Heure*, BIH), as well as in the *Astronomical Almanac* (1994, K10, B60). Appendix D shows other sources, and Table 1-7 shows some recent values. The actual displacements are given in arcseconds in the ***IERS Reference Meridian*** (IRM) direction ("x_p" measured positive south along the 0° longitude meridian) and the y_p meridian (90°W or 270°E meridian). The ***Celestial Ephemeris Pole*** (CEP) is the axis of Earth rotation, which is normal to the true equator. The ***International Reference Pole*** (IRP, formerly the *Conventional International Origin* (CIO) is the *mean* location of the pole agreed upon by international committees. It results from observed values between 1900 and 1905. Deflections locate the IRP from the CEP. The motion is roughly a circular spiral about the North Pole. The maximum amplitude of the variations is about 9 m in any direction. Figure 1-35 shows the geometry for the effect of polar motion.

pg 84 : Clarification and Correction

Figure 1-35. Transformation Geometry Due to Polar Motion. This transformation takes into account the actual location of the Celestial Ephemeris Pole (CEP) over time. It moves from an *ECEF* system without polar motion about the CEP, to an *ECEF* system with polar motion using the IERS Reference Pole (IRP). This displacement is very small, but highly accurate studies should include it especially when precise station location information is desired. The inset plot shows the motion of the IRP for about 10 years.

$$\Delta\phi_{gd} \approx x_p \text{COS}(\bar{\lambda}) - y_p \text{SIN}(\bar{\lambda})$$

$$\Delta\lambda \approx \left\{ x_p \text{SIN}(\bar{\lambda}) - y_p \text{COS}(\bar{\lambda}) \right\} \text{TAN}(\bar{\phi})$$

pg 87 : Clarification and Correction

$$T_{TDT} = \frac{JD_{TDT} - 2{,}451{,}545.0}{36{,}525} = \frac{2{,}448{,}352.828\,085\,303\,2 - 2{,}451{,}545.0}{36{,}525} = -0.087\,396\,904$$

pg 88-89 : Correction

$$\vec{r}_{ECItod} = 5119.280\,828\,5\,\hat{I} + 6113.238\,564\,7\,\hat{J} + 6374.070\,520\,8\,\hat{K} \text{ km}$$

$$\vec{v}_{ECItod} = -4.737\,180\,63\,\hat{I} + 0.799\,366\,73\,\hat{J} + 5.537\,765\,929\,\hat{K} \text{ km/s}$$

Determine the *GST* using the JD_{UT1}, Eq. (1-44), and Eq. (1-45):

$GST = 312.297\,677\,780\,19°$.

Find the *AST* using

$$\theta_{AST} = \theta_{GST} + \Delta\Psi\cos(\epsilon) = 312.301\,518\,154\,51°$$

After doing the rotation for sidereal time, you'll get these initial *ECEF* vectors:

$$\vec{r}_{ECEF\text{w/o}PM} = -1120.361\,147\,\hat{I} + 7894.524\,232\,0\,\hat{J} + 6374.070\,520\,8\,\hat{K} \text{ km}$$

$$\vec{v}_{ECEF\text{w/o}PM} = -3.187\,097\,89\,\hat{I} - 2.905\,170\,52\,\hat{J} + 5.537\,659\,29\,\hat{K} \text{ km/s}$$

Finally, determine polar motion. Find the x_p and y_p coefficients from Table 1-7 as x_p = –0.217" and y_p = 0.281". Actual daily values from USNO's IERS final data are x_p = –0.2206" and y_p = 0.3014". The approximate values in Table 1-7 are often adequate. Convert to radians and rotate for polar motion to find the final Earth-centered, Earth-fixed coordinates as

$$\vec{r}_{ECEF\text{w}PM} = -1120.367\,964\,1\,\hat{I} + 7894.514\,918\,0\,\hat{J} + 6374.080\,858\,3\,\hat{K} \text{ km}$$

$$\vec{v}_{ECEF\text{w}PM} = -3.187\,097\,89\,\hat{I} - 2.905\,170\,52\,\hat{J} + 5.537\,651\,63\,\hat{K} \text{ km/s}$$

.

---

pg 89 : Clarification

RMS magnitudes from the previous vector are listed in meters. The effect of precession becomes larger as the epoch date recedes from Jan 1, 2000. If this example were in 1998, the precession delta would be about 5000 m. This shows the relative effect of each change.

---

pg 90 : Wording

the angular difference between observations from the center of the Earth and those from a

---

pg 94 : Clarification

centric frames determined from VLBI measurements, whereas ***terrestrial frames*** are bound to the Earth. We'll mainly use terrestrial frames for the satellite motions in this book. The suggested Earth reference frame is the *International Terrestrial Reference Frame* (ITRF) model described by McCarthy (1992). Each revision is designated with a two-digit year (ITRF-94, ITRF-96). These reference frames are a particular definition of the FK5 system. As mentioned earlier, many datums further define terrestrial refere

---

pg 96 : Correction

conversion constants of the input and output routines. Routines that do the actual mathematical operations *remain unchanged!* The table on the inside back cover lists the defined

TABLE 1-6. Summary of J2000 Reduction Values for Example 1-6. This table shows the position and velocity vectors after each transformation. The main difference occurs with the correction for sidereal time—the transition between Earth-fixed and true coordinates. The terminology for mean and true values is not always followed. Mean equinox values are sometimes substituted for the true values listed.

Position (km)	$\hat{I}$	$\hat{J}$	$\hat{K}$	**Terminology**
	5102.509 600 00	6123.011 520 00	6378.136 300 00	$\vec{r}_{J2000}$, mean equator and mean equinox of J2000
Precession 20,503*	5119.880 902 16	6113.022 741 15	6373.795 530 72	$\vec{r}_{ECImod}$, mean equator and mean equinox of date
Nutation 689*	5119.280 828 5	6113.238 564 7	6374.070 520 8	$\vec{r}_{ECItod}$, true equator and true equinox of date
Sidereal time 6,448,090*	−1120.361 147 1	7894.524 232 0	6374.070 520 8	$\vec{r}_{ECEFw/oPM}$, *ECEF*
Polar motion 16*	−1120.367 964 1	7894.514 918 0	6374.080 858 3	$\vec{r}_{ECEFwPM}$, *ECEF*
Velocity (km/s)				
	−4.743 219 60	0.790 536 60	5.533 756 19	$\vec{v}_{J2000}$
Precession	−4.736 964 26	0.799 800 13	5.537 781 79	$\vec{v}_{ECImod}$
Nutation	−4.737 180 63	0.799 366 73	5.537 659 29	$\vec{v}_{ECItod}$
Sidereal time	−3.187 097 89	−2.905 170 52	5.537 659 29	$\vec{v}_{ECEFw/oPM}$
Polar motion	−3.187 097 89	−2.905 170 52	5.537 651 63	$\vec{v}_{ECEFwPM}$

*RMS magnitudes from the previous vector are listed in meters. The effect of precession becomes larger as the epoch date recedes from Jan 1, 2000. If this example were in 1998, the precession delta would be about 5000 m. This shows the relative effect of each change.

and derived constants of JGM-2. Again, be aware of the need for consistency between values in this table. Don't mix conversions from JGM-2, WGS-72, WGS-84, etc. when doing highly accurate studies. We can derive each value in the table from the other values.

2. The Astrodynamics division at Phillips Laboratory, located at ϕ_{gc} = 35.05°, λ = −106.40°, h_{ellp} = 1866.03 m, is located on the vernal equinox on May 2, 1996. What are the *LHA*$_{\Upsilon}$, *GHA*$_{\Upsilon}$, *LST*, and *GST*?

5. What are the J2000 position and velocity vectors for Example 1-6 in the *PQW*, *SEZ*, *RSW*, *NTW*, and *EQW* coordinate systems for a site at ϕ_{gd} = 40°N and λ = 100°W? Hint: Use ***ELORB*** (Algorithm 5) to find the orbital elements.

9. If the position and velocity vectors we determined in Example 1-6 (*ECEF*-wPM) are taken as mean-of-date values at the same epoch, what are the mean-of-date vectors on August 20, 1994? (Hint: Use one transformation only.)
10. Eq. (1-6) relates the vertical distance of a circle and an ellipse. What is the corresponding relation for a hyperbola?

Chapter 2.

pg 109 : Clarification

Notice if the sum of the time rate of change is zero, the quantity must be a constant. If we integrate both sides with respect to time, the differentials disappear, and the right-hand side also becomes a constant. The constant is called the *specific mechanical energy*, ξ. This equation is often referred to as the *energy integral*, or a form of the *vis-viva equation*. Rearranging then,

pg 110 : Clarification

The previous equations are sometimes combined to give an alternate formulation of the energy interval (Eq. (2-21) squared). This is the traditional form of the *vis-viva equation.*

pg 114 : Correction

(2) The period in the numerator is the number of TUs in one *sidereal* day, and it comes from the table on the inside back cover (1.0/0.009 363 658 228 3 = 106.795 869 7). Don't confuse this quantity with the TUs in one *solar* day (107.088 268 9).

pg 121-122 : Clarification

$$m_i \ddot{\vec{r}}_i = -G \sum_{i=1}^{n} \sum_{\substack{j=1 \\ j \neq i}}^{n} \frac{m_i m_j}{r_{ji}^3} \vec{r}_{ji}$$

pg 127 : Clarification

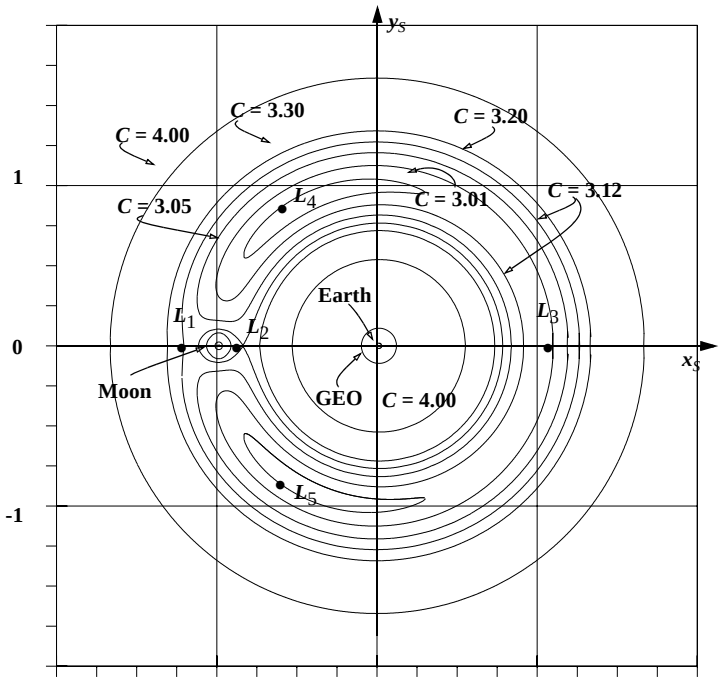

Figure 2-9. Regions of *x*-*y* Motion for the Earth-Moon System, $\mu^* = 0.012\,14$. This representation of motion in the Earth-Moon system shows the Lagrange points, as well as the positions of the Earth and Moon. A geosynchronous orbit is shown about the Earth to give a sense of scale. Notice the significant differences from Fig. 2-10 due to the smaller mass ratio of the Earth-Moon system. Motion across curves of lower *C* values is possible only with additional thrust.

pg 135 : Correction

subscript reminds us that these elements are valid for any orbit. Astronomers use two similar angles ($\tilde{\omega}$ and $\underline{\lambda_M}$) for real-world cases which approach the theoretical circular and equatorial orbits.

pg 136 : Correction

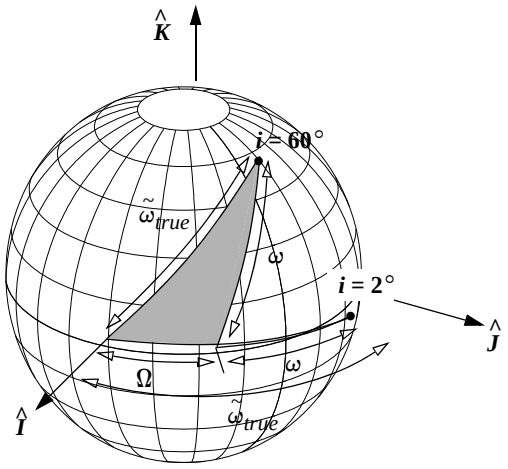

$i = 2°$, $e = 0.000\ 01$
$\Omega = 30°$, $\omega = 40°$
$\tilde{\omega}_{true} = 69.988\ 27°$

$i = 60°$, $e = 0.000\ 01$
$\Omega = 30°$, $\omega = 40°$
$\tilde{\omega}_{true} = 59.820\ 08°$

Figure 2-13. Representation of Longitude of Periapsis.

pg 141 : New Information

We find the estimated ballistic coefficient using Eq. (2-61) and $BC = 745.397\ 95\ kg/m^2$. As an aside, you may notice that the satellite is always near the equator at the epoch time. That's because the epoch is chosen to coincide with the ascending node *prior* to the last observation used in the differential correction (Chap. 9). Numerical vectors usually place the epoch at the last observation time.

pg 144 : Correction

$$\begin{aligned}
\lambda_M &= M + \omega + \Omega \\
g_p &= \sqrt{2(\sqrt{\mu a}(1-\sqrt{1-e^2}))}\,\mathrm{SIN}(\omega+\Omega)\,\mathrm{COS}(\omega+\Omega) \\
h_p &= \sqrt{2(\sqrt{\mu a(1-e^2)}(\mathrm{COS}(i)-1))}\,\mathrm{SIN}(\Omega)\,\mathrm{COS}(\Omega) \\
L_p &= \sqrt{\mu a} \\
G_p &= -\sqrt{2(\sqrt{\mu a}(1-\sqrt{1-e^2}))}\,\mathrm{SIN}(\omega+\Omega) \\
H_p &= -\sqrt{2(\sqrt{\mu a(1-e^2)}(\mathrm{COS}(i)-1))}\,\mathrm{SIN}(\Omega)
\end{aligned} \qquad (2\text{-}64)$$

pg 147 : Correction

$$\mathrm{COS}(\lambda_{true}) = \frac{r_I}{|\vec{r}|} \qquad \mathrm{IF}(r_J < 0)\,\mathrm{THEN}\ \lambda_{true} = 360^\circ - \lambda_{true}$$

$$\vec{e} = \frac{1}{\mu}\left[\left(v^2 - \frac{\mu}{r}\right)\vec{r} - (\vec{r}\cdot\vec{v})\vec{v}\right] = -0.3146\hat{I} - 0.385\,23\hat{J} + 0.668\,04\hat{K}$$

$$e = 0.832\,853$$

$$\xi = \frac{v^2}{2} - \frac{\mu}{r} = \frac{0.967\,936^2}{2} - \frac{1}{1.796\,23} = -0.088\,273\ \mathrm{ER}^2/\mathrm{TU}^2$$

$$p = \frac{h^2}{\mu} = \frac{1.317\,386^2}{1} = 1.735\,272\ \mathrm{ER} = 11{,}067.790\ \mathrm{km}$$

pg 153 : Correction

d. $\vec{h} = -3.5\hat{K}\ \mathrm{ER}^2/\mathrm{TU}$

On May 5, 2000, the seven inner planets will be *somewhat* aligned. Does this present another opportuniuty to "tour" the planets? Explain your answer. (Review question 9 before answering)

Chapter 3.

pg 159 : Wording

These routines convert times in an hour-minute-second (*HMS*) format to one in radians and vice versa. As with the *DMS* routines, ***HMStoRad*** contains only one equation which carries out the operation; however, recall the basic relations in Eq. (1-41):

pg 165 : Correction

.

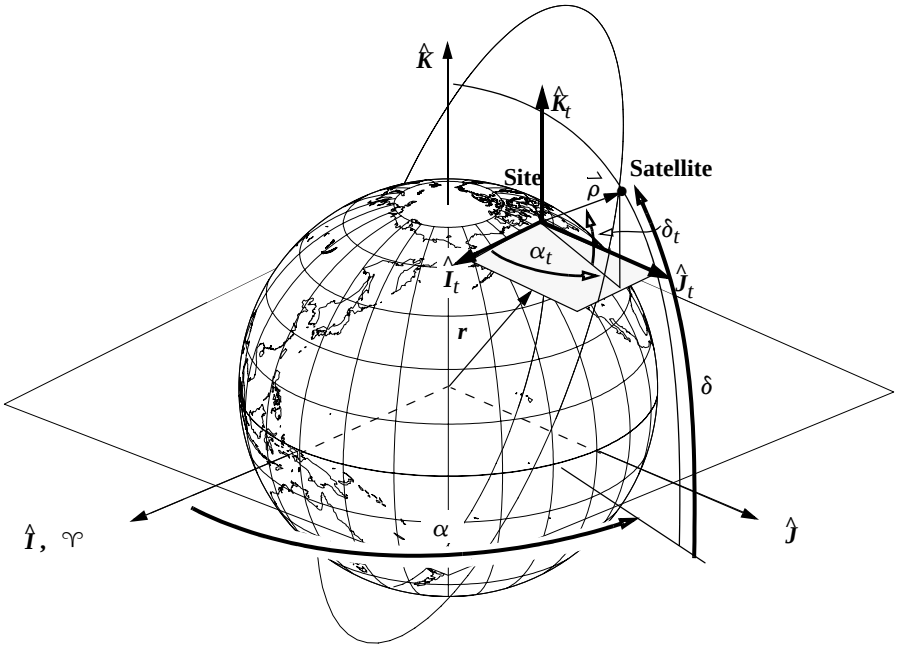

Figure 3-1. Right Ascension and Declination. Standard right ascension and declination use the Earth's equatorial plane. Topocentric right ascension and declination values use a plane parallel to the Earth's equator but located at a particular site. Transformations rely on determining the slant-range vector ($\hat{\rho}$) in the *IJK* system.

---

pg 179 : Correction

$\underline{\phi_{gd}} = 39.007°,\ \lambda = -104.883°,\ h_{ellp} = 2194.56$ m

$$\vec{r}_{siteIJK} = \begin{bmatrix} 4066.716 \\ -2847.545 \\ 3994.302 \end{bmatrix} \text{ km} = \begin{bmatrix} 0.6376 \\ -0.4464 \\ 0.6262 \end{bmatrix} \text{ ER}$$

---

pg 183 : Correction

GIVEN: April 2, 1994, 0:00 *UT*1

---

pg 187 : Correction

GIVEN: April 28, 1994, 0:00 *UT*1

---

pg 190 : Correction

From Table D-4, find values for the orbital elements of Jupiter. These values allow you to find the heliocentric elements for the mean equator, mean equinox of J2000. Remember that these equations differ from the mean of date values listed on page 189.

$$a = 5.202\,603\,191 + 1.913\times10^{-7} T_{TDB} = 5.202\,603 \text{ AU}$$

$$e = 0.048\,494\,85 + 0.000\,163\,244 T_{TDB} - 4.719\times10^{-7} T_{TDB}^2 - 1.97\times10^{-9} T_{TDB}^3$$
$$= 0.048\,486$$

$$i = 1.303\,270° - 0.001\,987\,2 T_{TDB} + 3.318\times10^{-5} T_{TDB}^2 + 9.2\times10^{-8} T_{TDB}^3$$
$$= 1.303\,382°$$

$$\Omega = 100.464\,441° + 0.176\,682\,8 T_{TDB} + 0.000\,903\,87 T_{TDB}^2 - 7.032\times10^{-6} T_{TDB}^3$$
$$= 100.454\,519°$$

$$\tilde{\omega} = 14.331\,309° + 0.215\,552\,5 T_{TDB} + 0.000\,722\,52 T_{TDB}^2 - 4.59\times10^{-6} T_{TDB}^3$$
$$= 14.319\,203°$$

$$\lambda_M = 34.351\,484° + 3034.905\,674\,6 T_{TDB} - 0.000\,085\,01 T_{TDB}^2 + 4.0\times10^{-9} T_{TDB}^3$$
$$= -136.123\,94°$$

$$M = \lambda_M - \tilde{\omega} = -150.443\,142°$$

$$\omega = \tilde{\omega} - \Omega = -86.135\,316°$$

KEPEQTNE $(M, e \Rightarrow \nu)$, $\nu = \underline{206.954\,53}°$

Because the numbers are very large when we convert to km and km/s, the answer is often left in AU and AU/TU. A simple rotation produces the geocentric vector, still referencing the mean equator and mean equinox of J2000. Use Eq. (1-58) to find $\underline{\epsilon}$.

pg 194 : Font

the site and the Sun, ς, shown in Fig. 3-8

pg 195-7 : Correction

$$JD_{sunrise} = JD_{0h} + 6\text{ h}/24\text{ h/day} - \lambda/\underline{360}^{\circ}/\text{day}$$

$$JD_{sunset} = JD_{0h} + 18\text{ h}/24\text{ h/day} - \lambda/\underline{360}^{\circ}/\text{day}$$

pg 204-205 : Correction

$$\text{SIN}(\delta) = \frac{r_{Ksat}}{r} \quad \text{or} \quad \text{TAN}(\delta) = \frac{r_{Ksat}}{r_{\delta sat}}$$

Let $\phi_{gd} = \delta \qquad r_{\delta} = r_{\delta sat} \qquad r_K = r_{Ksat}$

$\lambda = \alpha - \theta_{GST} = -287.447\,086^{\circ} = 72.\underline{5529}^{\circ}\underline{\text{E}}$

$r_{\delta sat} = \sqrt{r_I^2 + r_J^2} = 1.4847\text{ ER}$

$\text{SIN}(\alpha) = \frac{r_J}{r_{\delta sat}} \qquad \alpha = 46.4464^{\circ} \qquad \text{TAN}(\delta) = \frac{r_{Ksat}}{r_{\delta sat}} \qquad \delta = 34.2527^{\circ}$

$\text{TAN}(\phi_{gd}) = \frac{r_K + C_{\oplus} e_{\oplus}^2 \text{SIN}(\phi_{gd})}{r_{\delta}} \Rightarrow \phi_{gd} = 34.352\,242,\ 34.352\,495,\ 34.352\,496$

Chapter 4.

pg 214 : Correction

A single equation for true anomaly is useful. Divide Eq. (4-12) by Eq. (4-10) and use the tangent half-angle formula to expand the result:

pg 222 : Correction

A single equation for true anomaly is useful. Dividing Eq. (4-33) by Eq. (4-31) provides a tangent expression. Use the formula for the tangent half-angle to expand the result:

pg 249 : Correction

ELORB ($\vec{r}_o, \vec{v}_o \Rightarrow a, e, i, \Omega, \omega, \nu(u, \lambda_{true}, \tilde{\omega}_{true})$)

IF $e \neq 0$

***ν*toAnomaly** ($e, \nu \Rightarrow E_o, B_o, H_o$)

ELSE

$E_o = u$ or $E_o = \lambda_{true}$

if $e < 1.0$	if $e = 1.0$	if $e > 1.0$
$M_o = E_o - e\text{SIN}(E_o)$	$\vec{h} = \vec{r}_o \times \vec{v}_o$	$M_o = e\text{SINH}(H_o) - H_o$
$M = M_o + n\Delta t$	$p = \frac{h^2}{\mu}$	$M = M_o + n\Delta t$
KepEqtnE ($M, e \Rightarrow E$)	$M_o = B_o + \frac{B_o^3}{3}$	***KepEqtnH*** ($M, e \Rightarrow H$)
	KepEqtnP($\Delta t, p \Rightarrow B$)	

pg 250 : Clarifcation

Because the last cross product is zero and the first has a value only in the $\hat{W}$ direction, you can consider the term multiplying f as a magnitude. Also, recognize that this term ($\vec{r}_o \times \vec{v}_o$) is the angular-momentum. Therefore,

pg 251 : Clarifcation

We can also adopt a matrix notation and write the update in Eq. (4-57) as a state vector of position and velocity vectors, and with Φ as a matrix containing *scalar* 3×3 matrices (See Sec. C.2) of the f and g values.

pg 254 : Correction

$$\vec{r}(\tau) = \vec{r}(t) + \dot{\vec{r}}(t)\tau + \frac{\ddot{\vec{r}}(t)\tau^2}{2!} + \frac{\dddot{\vec{r}}(t)\tau^3}{3!} + \ldots$$

pg 262 : Correction

$$\dot{g} = 1 - \frac{\chi_n^2}{r} c_2 \qquad \dot{f} = \frac{\sqrt{\mu}}{r r_o} \chi_n (\psi c_3 - 1)$$

pg 263 : Correction

Iterate to get the values shown in 4-4:

TABLE 4-4. Values for Kepler's Problem in Example 4-4. Iteration values are shown. Notice how quickly we arrive at the correct answer.

Iteration	χ_n	ψ	r	χ_{n+1}
1	2.634 916	6.149 802	1.136 164	2.640 192
2	2.640 192	6.174 452	1.136 192	2.640 192

$$f = 1 - \frac{\chi_n^2}{r_o} c_2 = -0.806\,637 \qquad g = \Delta t - \frac{\chi_n^3}{\sqrt{\mu}} c_3 = 0.726\,406\,9$$

$$\dot{g} = 1 - \frac{\chi_n^2}{r} c_2 = -0.780\,550 \qquad \dot{f} = \frac{\sqrt{\mu}}{r r_o} \chi_n (\psi c_3 - 1) = -0.509\,878$$

pg 266 : Correction

We can also determine an approximate value for the semimajor axis from the groundtrack. We first find the orbital period and then a, using Eq. (2-19). The change in longitude, $\Delta\lambda$ measured from the initial starting location, in one revolution gives us the satellite's period,

pg 271 : Correction

5. A certain groundtrack is noticed with a regular 25° westward displacement on each rev. What is the semimajor axis? How can you be sure?

Chapter 5.

pg 277 : Correction

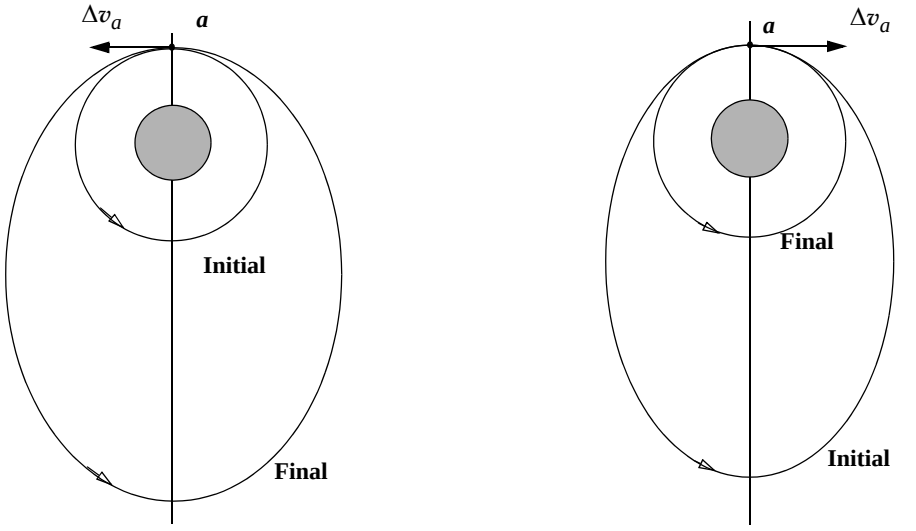

Figure 5-2. Tangential Orbit Transfer ($\phi_{fpa} = 0°$). Tangential burns are defined to occur with a zero flight-path angle. Velocity increases enlarge the semimajor axis (left), whereas decreases cause the orbit to come closer to the Earth (right).

pg 286 : Correction

pg 288-289 : Correction

Figure 5-7. One-Tangent Burns. For both circular (left) and elliptical (right) orbit changes, the true anomalies of the transfer and final orbits are equal. The maneuver starts at apoapsis (left, $\nu > 180°$) and periapsis (right, $\nu < 180°$) of the transfer orbit.

Notice that ν_{trans_b} is usually less than 180° for transfers that begin at perigee. It's usually larger than 180° for transfers that begin at apogee. All solutions have two answers—the other is at $360° - \nu_{trans_b}$ —the only difference is the time because Δv is the same.

What difference, if any, must take place if the tangential burn occurs at apoapsis and not periapsis? The change in velocity must be in the opposite direction and reformulated

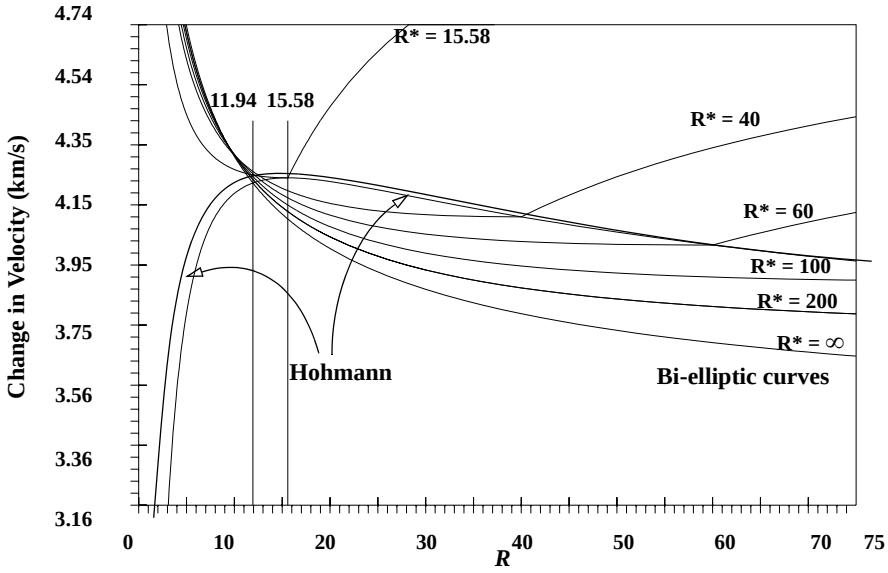

Figure 5-6. Hohmann Transfer—Comparison of Change in Velocity. The change in velocity

because now apoapsis is the first burn location. Besides the general restriction on ν based on the origin of the manuever, the values of true anomaly are also limited. By solving for the denominator of Eq. (5-10), we see that the true anomaly must obey the following restriction to avoid parabolic solutions [numerical indeterminacy]. We determine the signs opposite from Eq. (5-10):

---

pg 293 : Clarification

Coplanar maneuvers enable a satellite to alter three orbital elements: semimajor axis, eccentricity, and argument of perigee. To do an intercept or rendezvous, we may need to

---

pg 295 : Correction

ciable. Using data from the table on the inside back cover, we find the velocity for a site at the equator is

---

pg 300 : Wording

The inclination-only maneuver is a very simple operation. If the change in velocity is important, be sure to check *both* nodes and use the node with the smaller initial velocity.

For circular orbits, there will be no difference. The flight-path angle is necessary for elliptical orbits.

---

pg 308 : Correction

Because you don't know the best values for the change in inclination at each location, identify each using a scaling term, *s*, that represents a percentage of the initial (or first) inclination change ($\Delta i_{initial} = s\Delta i$, $\Delta i_{final} = (1 - s)\Delta i$).

$$\Delta v = \Delta v_a + \Delta v_b = \sqrt{v_{initial}^2 + v_{trans_a}^2 - 2v_{initial}v_{trans_a}\cos(s\Delta i)} + \sqrt{v_{final}^2 + v_{trans_b}^2 - 2v_{final}v_{trans_b}\cos((1-s)\Delta i)}$$

$$\Delta v_a^2 + \Delta v_b^2 \approx v_{initial}^2 + v_{trans_a}^2 - 2v_{initial}v_{trans_a}\cos(s\Delta i) + v_{final}^2 + v_{trans_b}^2 - 2v_{final}v_{trans_b}\cos((1-s)\Delta i)$$

---

pg 327 : Correction

$\Delta v_{trans2}^2 = v_{trans2}^2 + v_{tgt}^2 - 2v_{trans2}v_{tgt}\cos(\Delta i) = 0.228\ 003$ ER/TU

Finally, the total Δv is

S $\Delta v_{TOTAL} = \Delta v_{phase} + \Delta v_{trans1} + \Delta v_{trans2}$, = 0.518 803 ER/TU = 4.101 329 km/s.

---

pg 336 : Correction

the table on the inside back cover for the physical constants.

---

pg 337 : Correction

---

pg 352 : Correction

GIVEN: The Hubble Space Telescope is about to be released from the Space Shuttle, which is in a circular orbit at 590 km altitude. The relative velocity (from the Space Shuttle bay) of the ejection is 0.1 m/s down, 0.04 m/s backwards, and 0.02 m/s to the right.

FIND: Position and velocity of the Hubble Space Telescope after 5 and 20 minutes.

First, convert the given data to the correct sign convention for the relative motion definitions. The initial velocities are then

$\dot{x}_o = -0.1 \qquad \dot{y}_o = -0.04 \qquad \dot{z}_o = -0.02$ m/s

---

pg 354 : Correction

$$z = D\cos(\omega t - \phi_o) \tag{5-52}$$

---

pg 355 : Clarification

Figure 5-26. Interceptor's Instantaneous Relative Motion about the Target. We can define an elliptical region in which the interceptor "orbits" about the target satellite. (This is similar to a prolate spheroid, discussed in Sec. 1.3.2.) Although it's not actually an orbit, we can approximate the motion as an ellipse for short time spans. Over time, this instantaneous figure stretches (due to the $\dot{y}_c$ drift term) into an elliptic cylinder that encompasses the satellites motion. Also recognize that this is really an irregular ellipsoidal region and is exaggerated in this figure. The periodic curves are illustrative and aren't representative of actual motion.

---

pg 356-357 : Clarification and Correction

Varying the interceptor's initial conditions gives us several interesting motions including straight lines. $\dot{y}_o = 0.044\ 15$ m/s for x_o negative, and $\dot{y}_o = -0.044\ 15$ m/s for x_o positive.

.

---

pg 365 : Correction

$\dot{z}_o = 0.0359$ m/s $\qquad\qquad \dot{z}_o = 0.0082$ m/s

---

pg 369 : Correction

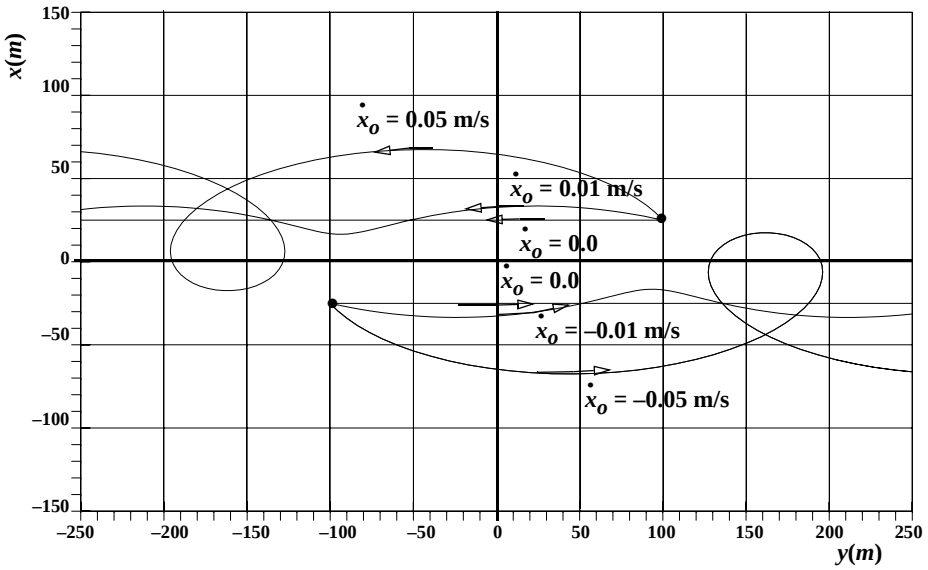

Figure 5-27. Motion of the Interceptor for Various x_o Displacements. Notice how all displacements above the satellite move to the left (lower velocity causes a lagging effect), whereas those below move to the right (higher velocity causes a lead). In addition, as the satellite's initial location gets farther from the target, the motion away from the target increases.

final parking orbit. Assume the solid rocket motors place the Shuttle at apogee of a 0 km by 110 km altitude orbit. The Shuttle then uses a 110 km by 300 km Hohmann transfer orbit to achieve the final orbit (300 km by 300 km). If the Shuttle remains in each orbit for

Chapter 6.

pg 377 : Correction

$$f_d = -\frac{2\dot{\rho}}{\lambda}$$

pg 391 : Correction

Because we have to make an initial guess for the middle radius, we must iterate to determine the final value for ρ. Escobal ([1965] 1985, 264–265) presents an approach, as do Baker and Makemson (1967, 134). Substituting Eq. (6-11) into Eq. (6-6) results in

pg 406-407 : Clarification

determination in the NASA-sponsored research of Smith and Huang, is of particular interest. We wish to find $\boldsymbol{X}$ such that $f(\boldsymbol{X}) = \boldsymbol{b}$. Let $\underline{\boldsymbol{X}_1}$ be an initial guess and put $\underline{\boldsymbol{b}_1 = f(\boldsymbol{X}_1)}$. Put $\underline{\boldsymbol{b}_i = \boldsymbol{b}_{i-1}}$ and for each real number λ put

$$\boldsymbol{b}_\lambda = (1-\lambda)\boldsymbol{b}_{i-1} + \lambda \boldsymbol{b}_i$$

We'll seek a continuous family $(\boldsymbol{X}_\lambda)$ of solutions to $f(\boldsymbol{X}_\lambda) = \boldsymbol{b}_\lambda$. Note that any solution corresponding to $\lambda = 1$ is a solution to our original equation.

Differentiating with respect to a parameter s (which is the arc length from $\underline{\boldsymbol{b}_i}$) yields

$$\frac{\partial f}{\partial \boldsymbol{X}} \frac{d\boldsymbol{X}}{ds} = (\boldsymbol{b}_i - \boldsymbol{b}_{i-1})\frac{d\lambda}{ds}$$

or in matrix form,

$$\left[\frac{\partial f}{\partial \boldsymbol{X}} \; (\boldsymbol{b}_{i-1} - \boldsymbol{b}_i)\right] \begin{bmatrix} \dfrac{d\boldsymbol{X}}{ds} \\ \dfrac{d\lambda}{ds} \end{bmatrix} = 0$$

pg 424 : Clarification

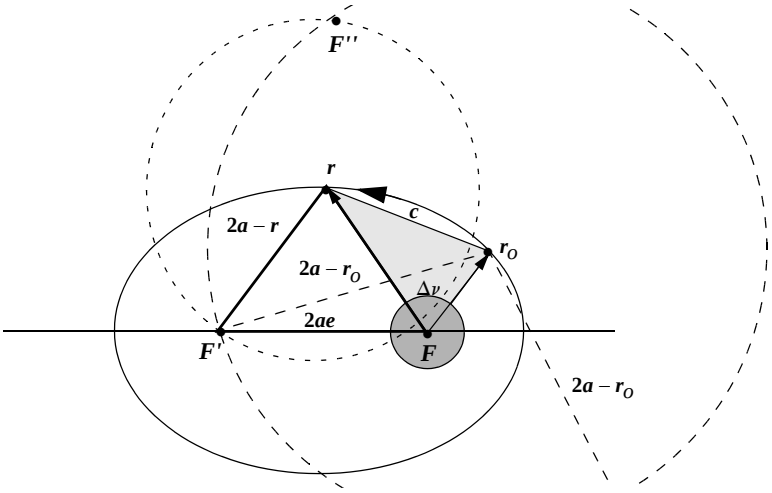

Figure 5-28. Geometry for the Lambert Problem (I). This figure shows how we locate the secondary focus—the intersection of the dashed circles. The chord length, *c*, is the shortest distance between the two position vectors. The sum of the distances from the foci to any point, *r* or r_o, is equal to twice the semimajor axis.

pg 429 : Clarification

Thorne has developed an important and useful series solution to the Lambert problem [Thorne and Bain (1995)]. It's equally valid for hyperbolic and elliptical transfer times that are less than the time for minimum-energy transfer. As shown earlier, the transfer t

pg 430 : Correction

$$Q_{1,1} = A_1^{-1}$$

$$Q_{i,j} = \sum_{k=1}^{i-1} Q_{i-k,j-1}\, Q_{k,1} \qquad (i = 2, 3, 4, \ldots),\ 1 < j \le i \tag{6-42}$$

$$Q_{i,1} = \sum_{k=1}^{i-1} \left(\frac{-1}{A_1}\right) Q_{i,k+1}\, A_{k+1}$$

pg 449 : Clarification

.

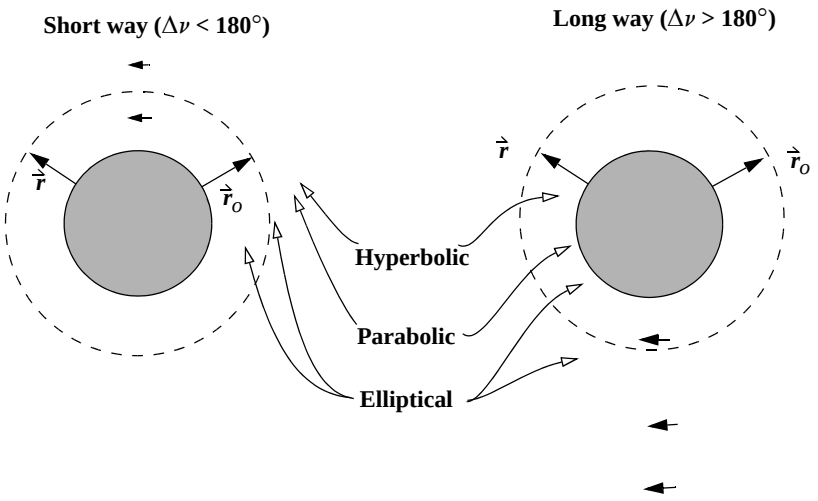

Figure 6-16. Varying Time of Flight for Intercept. As the time of flight increases for the transfer to the target (short way left, long way right), the transfer orbit becomes less eccentric until it reaches a minimum, shown as a dashed line. The eccentricity then begins to increase after this transfer. There is always a minimum eccentricity transfer, and a minimum change in velocity transfer. However, they generally don't occur at the same time. Finally, I've shown the initial and final positions with the same magnitude. This is not an additional requirment.

pg 450 : Correction.

IF $((\hat{r}_{int} \cdot \hat{v}_{trans_a}) < 0.0)$ and $((\hat{r}_{tgt} \cdot \hat{v}_{trans_b}) > 0.0)$

pg 455-456 : Correction.

t.

normal vector for the transfer orbit $(Tran_n = \hat{r}_{int} \times \hat{r}_{tgt})$ and for the interceptor orbit prior to the burn $(\hat{h}_n = \hat{r}_{int} \times \hat{v}_{int})$. Then,

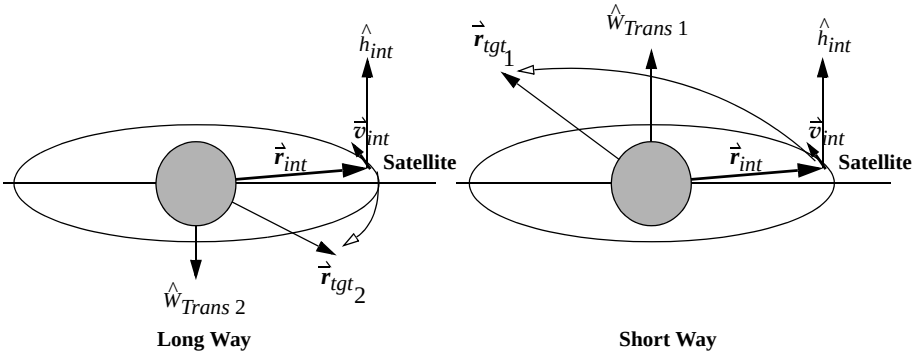

Figure 6-17. Orbital Geometry Showing Transfer Direction. We can determine if we're going the "shortest" way to the target by using cross products. The short-way trajectory is used when the interceptor angular momentum vector, h_{int}, is in the same direction as the transfer unit vector, $W_{Trans\ 1}$. The long way results when h_{int} and $W_{Trans\ 2}$ are in opposite directions.

---

pg 460-461 : Correction.

Axis legends for both figures (6-25 and 6-26) for the Transfer TOF are incorrect. They should range from 0 to 100 minutes, by 20 minutes.

---

pg 462 : New Information

6. Use the following data to determine the position of a newly discovered asteroid. The data is from MSSS during a preliminary collection on asteroids. Be careful of the units because this problem is solved with AU's. Are parallax and reduction techniques necessary? Hint: see Table 9-1 for the location of MSSS, and be sure to use the transformations in Chap. 3 to preprocess the data.

Year	Month	Days (*UTC*)	α_t (h min sec)	δ_t (° ' '')
1995	March	17.435 38	11 00 57.79	5 31 19.7

---

pg 463 : Correction

Year	Month	Days (*UTC*)	α_t (h min sec)	δ_t (° ' '')

Chapter 7.

pg 481 : Correction

$$\hat{S}^{\mathrm{I}}_{n-1} = \frac{1}{h}\ddot{\hat{r}}_{n-1} - \left\{\frac{1}{2}\ddot{\hat{r}}_{n-1} + \alpha_{AM2}\nabla(\ddot{\hat{r}}_{n-1}) + \alpha_{AM3}\nabla_2(\ddot{\hat{r}}_{n-1}) + \alpha_{AM4}\nabla_3(\ddot{\hat{r}}_{n-1}) + \ldots\right\}$$

$$\hat{S}^{\mathrm{II}}_{n-1} = \frac{1}{h}\ddot{\hat{r}}_{n-1} - \left\{\frac{1}{12}\ddot{\hat{r}}_{n-1} + \alpha_{C2}\nabla(\ddot{\hat{r}}_{n-1}) + \alpha_{C3}\nabla_2(\ddot{\hat{r}}_{n-1}) + \alpha_{C4}\nabla_3(\ddot{\hat{r}}_{n-1}) + \ldots\right\}$$

pg 486 : Clarification

pg 490 : Clarification

pg 492 : Clarification

We can also separate the zonal and tesseral terms from Eq. (7-17) by recalling that $J_\ell = -C_{\ell,0}$ [Eq. (1-13)]. The minus sign for the zonal harmonic coefficients is purely conventional, as described in Chap. 1 (Sec. 1.3). Thus,

pg 494 : Correction

strongest perturbation due to the Earth's shape. As the table on the inside back cover shows, J_2 is almost 1000 times larger than the next largest coefficient (J_3). Each of the

pg 498 : Correction

bility to drag forces. The drag coefficient for satellites in the upper atmosphere is often considered to be approximately $c_D \sim 2.2$ (flat plate). Spheres have $c_D \sim 2.0$ to 2.1. The drag coefficient is configuration-specific and is seldom approximated to more than three

pg 517 : Wording

If we assume the usual convention of a column representation for a vector, then the exterior product of two vectors is defined as the product of an $n \times 1$ column vector with a $1 \times m$ row vector, which results in an $n \times m$ matrix. We use this notation to represent our result. Evaluation of the partial derivatives in Eq. (7-35) yields

Like drag, solar-radiation pressure is a nonconservative perturbation, but it becomes important at somewhat higher altitudes. One of the more difficult aspects of analyzing solar radiation is accurately modeling and predicting the solar cycles and variations. Dur

---

pg 518 : Correction

$$p_{SR} = \frac{1353}{3\times10^8}\frac{\mathrm{W/\,m^2}}{\mathrm{m/s}} = 4.51\times10^{-6}\frac{\mathrm{W\cdot s}}{\mathrm{m^3}} = 4.51\times10^{-6}\frac{\mathrm{N}}{\mathrm{m^2}}$$

---

pg 519-522 : Correction and rework

---

pg 522 : Wording

Solution of the quartic is analytical and will yield the desired values of true anomaly for entry and exit. We know that the shadow occurs when ς is greater than 90°, thus COS(ς) in Eq. (7-41) must be less than zero. We can determine if it's an entry or an exit using Eq. (7-42). For example, if the shadow function, *S*, is changing from negative to positive, it's an entry. Numerical computations show that, typically, only one real root will satisfy the requirements for our problem. If there is more than one root, we need additional logic.

---

pg 526 : Clarification

$$U = \frac{\mu}{r}\left[1 + \sum_{\ell=2}^{\infty}\sum_{m=0}^{\ell}\left(\frac{R_\oplus}{r}\right)^{\ell} P_{\ell m}[\mathrm{SIN}(\phi_{gc_{sat}})]\left\{C_{\ell m}\mathrm{COS}(m\lambda_{sat}) + S_{\ell m}\mathrm{SIN}(m\lambda_{sat})\right\}\right]$$

$$U_{2\text{-}body} = \frac{\mu}{r}$$

$$\grave{a}_{nonspherical} = \nabla(U - U_{2\text{-}body}) = \nabla R$$

---

pg 531 : Clarification

For computer implementation, remember that *m* represents the order of the derivative. If *m* is larger than ℓ, the derivative value is zero because the ℓth derivative is always one. This affects only $P_{\ell-2,m}[\alpha]$. We sum ℓ from 2 to the order desired, and then *m* goes from 0 to ℓ. Remember to initialize each calculation with $P_{0,\ell-1} = 0$. We'll see later that resonance

pg 533 : New Information

time-varying attitudes. ***Macro models*** help in that they try to piece together well-known shapes to approximate the satellite's true shape. They're especially useful for drag and solar-radiation calculations. Luthcke et al. (1997) used a macro model for TDRS to improve the orbit determination accuracy to a few meters. Getting the satellite's precise orientation is equally difficult and, in many cases, may actually involve commanding and controlling the satellite to receive health and status information from it.

pg 534 : New Information

wealth of information for any validation effort. Be careful to use the same databases when using different systems. It's especially difficult to ensure atmospheric databases have identical actual and predicted values for systems that use automatic update software.

pg 535 : Correction, New Information

the table on the inside back cover, the speed of light, masses of the planets, a sea-surface model, etc. We *must use a complete and consistent set of physical*

In this light, Vetter (1994) recommends the JGM-2 (Nerem et al., 1994) and the newer JGM-3 models because they're derived from many orbit classes. The EGM-360 effort is developed among the University of Texas at Austin, the Defense Mapping Agency, Ohio State University, and the Goddard Spaceflight Center. The model uses data from 30 satellites and from surface gravity measurements; it is a complete 360 × 360 field. These most accurate models are available from the main developers at the University of Texas at Austin and the Goddard Spaceflight Center. See Appendix D.5, "Data Sources," for the complete address. Any of these gravity fields may be *tuned* for a particular orbit, although tuning is uncommon because it's complex.

pg 536 : New Information

coordinates are available from several sources. The U.S. Naval Observatory provides access by Internet to obtain timing and pole-position data.

pg 537 : Wording

7. Program the Jacchia-Roberts model discussed in Appendix B, and compare the results to the exponential model for daily values in the months of January, 1986, and May, 1996. Explain differences and similarities. Hint: you'll need to obtain data using information in Appendix D.5.

Chapter 8.

pg 548 : Correction

The small parameters present may not all be of the same order of magnitude—for example, $J_2 \approx 10^{-3}$, $J_4 \approx 10^{-6}$, etc. Consequently, we should be careful to select the appropriate degree of each small parameter so all numerical contributions of a given order of magnitude are included. Hence, J_2^2 terms are often included in solutions when other zonal harmonic terms are included because $J_i \approx O(J_2^2)$; that is, the other zonal harmonic coefficients, J_3, J_4, J_5 are roughly of order J_2^2.

pg 568 : Correction

$$F_R = \frac{\mu}{r^2}\sum_{\ell=2}^{\infty} J_\ell\,(\ell+1)\left(\frac{R_\oplus}{r}\right)^\ell P_\ell\,[\mathrm{SIN}(i)\,\mathrm{SIN}(u)]$$

$$F_S = -\frac{\mu}{r^2}\mathrm{SIN}(i)\,\mathrm{COS}(u)\sum_{\ell=2}^{\infty} J_\ell\left(\frac{R_\oplus}{r}\right)^\ell P'_\ell\,[\mathrm{SIN}(i)\,\mathrm{SIN}(u)] \qquad (8\text{-}26)$$

$$F_W = -\frac{\mu}{r^2}\mathrm{COS}(i)\sum_{\ell=2}^{\infty} J_\ell\left(\frac{R_\oplus}{r}\right)^\ell P'_\ell\,[\mathrm{SIN}(i)\,\mathrm{SIN}(u)]$$

pg 569 : Clarification

is diagonal and the partial derivatives of the disturbing function are replaced by partial derivatives of the Hamiltonian. Also remember that the orbital elements (c_k) are a canonical set of variables.

pg 584 : Correction

$$\dot{M}_o = \frac{-3nR_\oplus^2 J_2\sqrt{1-e^2}}{4p^2}\left\{3\mathrm{SIN}^2(i)-2\right\} \qquad (8\text{-}41)$$

pg 585 : Correction

$$\dot{M}_o = \frac{3nR_\oplus^2 J_2\sqrt{1-e^2}}{4p^2}\{2-3\text{SIN}^2(i)\}$$
$$+\frac{3nR_\oplus^4 J_2^2}{512p^4\sqrt{1-e^2}}\left\{\begin{array}{l}320e^2-280e^4+(1600-1568e^2+328e^4)\text{SIN}^2(i)\\ +(-2096+1072e^2+79e^4)\text{SIN}^4(i)\end{array}\right\} \qquad (8\text{-}42)$$
$$-\frac{45J_4R_\oplus^4 e^2 n\sqrt{1-e^2}}{128p^4}\{-8+40\text{SIN}(i)-35\text{SIN}^2(i)\}$$
$$+\frac{35J_6R_\oplus^6 n\sqrt{1-e^2}}{2048p^6}\{-128+320e^2+240e^4+(1344-3360e^2-2520e^4)\text{SIN}(i)$$
$$+(-1512+3780e^2+2835e^4)\text{SIN}^2(i)-(-1848+4620e^2+3465e^4)\text{SIN}^4(i)\}$$

$$\Delta a_{SP} = \frac{J_2R_\oplus^2}{a}\left[\left(\frac{a}{r}\right)^3-\frac{1}{(1-e^2)^{3/2}}\right.$$
$$\left.+\left\{-\left(\frac{a}{r}\right)^3+\frac{1}{(1-e^2)^{3/2}}+\left(\frac{a}{r}\right)^3\text{COS}(2\omega+2\nu)\right\}\frac{3\text{SIN}^2(i)}{2}\right]$$

---

pg 590 : Correction

$$\dot{c} = \alpha+\beta\text{COS}(\omega_\oplus t)+\gamma\text{COS}\left(\dot{\omega}t\right)+\delta\text{COS}(nt)$$

---

pg 595 : Wording

The magnitude of these effects are usually larger than the short-periodic variations from the zonal harmonics. In fact, the magnitude of J_2 long-periodic effects can be very large. Consider the long-periodic change in a satellite's apogee location. Over an extended period of time, a site will see both perigee and apogee—a difference of 2*ae*. This can be several hundred kilometers! The remaining zonal harmonics produce oscillations that are much smaller in magnitude (by a factor of about 1000).

---

pg 598 : Correction

where *P* and *Q* are integers, and $Q \neq 0$. Those values of ℓ, *m*, *p* which satisfy the condition

$$\frac{P}{Q} = \frac{m}{\ell - 2p}$$

or $m = jP$, $jQ = (\ell - 2p)$, $j = 1, 2, 3, \ldots$ identify those terms in the Kaula potential with argument rates that nearly vanish. Such arguments are called critical arguments and are the source of resonance oscillations with very long periods. ***Anomalistic resonance*** is contributed by terms which satisfy $\ell - 2p = 0$ and $q \neq 0$. It's caused only by tesseral harmonics of even degree because of the constraint $\ell - 2p = 0$ for cases where the mean motion is commensurate with the Earth's rotation rate.

$$\dot{\Theta}_{\ell mpq} \approx 0 \Rightarrow q\dot{M} \approx m(\omega_{\oplus} - \dot{\Omega})$$

or $m = jP$, $jQ = q$, $j = 1, 2, 3, \ldots$

---

pg 599 : Clarification

and order of the tesseral-harmonic term. These higher-order harmonics for degree and order have smaller gravitational coefficients, $C_{\ell m}$ and $S_{\ell m}$, making the contributions less significant. In fact, P and Q may be so large that they determine unrealistically large values of ℓ and m or, at least, values for which the coefficients $C_{\ell m}$ and $S_{\ell m}$ aren't determined.

---

pg 600 : Clarification

Next, let's consider how we determine the integers P and Q. First, more than one pair $[P_i, Q_i]$ may satisfy the conditions. This assumes we've reduced P_i and Q_i to the lowest

---

pg 601 : Clarification

We can compute P_i and Q_i recursively by

---

pg 603 : Correction

.

---

pg 613 : Correction

$$\dot{e} = -\frac{15\mu_3 e\sqrt{1-e^2}}{4r_3^3 n}\{2AB\,\mathrm{COS}(2\omega) - (A^2 - B^2)\,\mathrm{SIN}(2\omega)\}$$

$$\dot{i} = \frac{3\mu_3 C}{4r_3^3 n\sqrt{1-e^2}}\{A[2 + 3e^2 + 5e^2\,\mathrm{COS}(2\omega)] + 5Be^2\,\mathrm{SIN}(2\omega)\} \qquad (8\text{-}43)$$

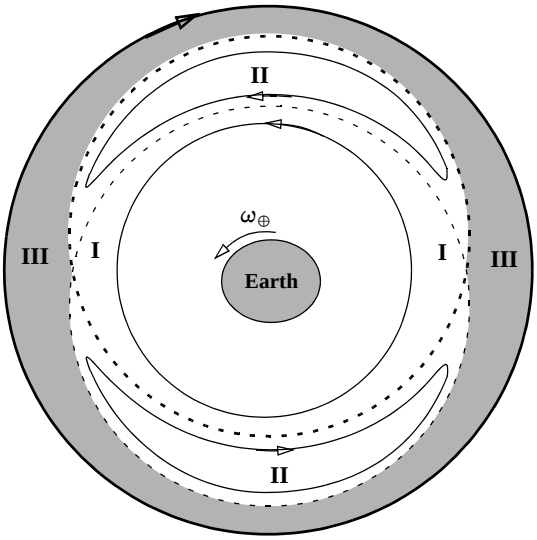

Figure 6-18. Motion of a Geosynchronous Satellite. Shows paths of nearly circular, small-inclination orbits in a coordinate frame rotating with Earth, as seen from the North Pole. Arrows show the satellite's direction of motion. Region I: orbital periods are less than 24 hr; Region II: periods are 24 hours; Region III: periods are greater than 24 hours.

$$\dot{\Omega} = \frac{3\mu_3 C}{4r_3^3 n\sqrt{1-e^2}\,\mathrm{SIN}(i)}\{5Ae^2\,\mathrm{SIN}(2\omega) + B[2 + 3e^2 - 5e^2\,\mathrm{COS}(2\omega)]\}$$

$$\dot{\omega} = -\dot{\Omega}\mathrm{COS}(i) + \frac{3\mu_3\sqrt{1-e^2}}{2r_3^3 n}\left\{5AB\,\mathrm{SIN}(2\omega) + \frac{5}{2}(A^2 - B^2)\,\mathrm{COS}(2\omega)\right.$$

$$\left. - 1 + \frac{3(A^2 + B^2)}{2}\right\} + \frac{15\mu_3 a(A\,\mathrm{COS}(\omega) + B\,\mathrm{SIN}(\omega))}{4r_3^3 n e r_3}\left[1 - \frac{5}{4}(A^2 + B^2)\right]$$

---

pg 621 : Clarification and Wording

(4.5×10^{-6} kg·m / s^2). These numbers don't match exactly due to the variability in atmospheric density. Highly accurate simulations often include solar radiation pressure effects to much lower altitudes.

Summary of Solar-Radiation Effects

1. Radiation pressure induces periodic variations in all orbital elements, exceeding the effects of atmospheric drag at heights above about 800 km. However, remember to include its effect for much lower altitudes.

It's important to realize that each averaging process will produce "mean" elements that are specific to that process. This is important because most analytical techniques use mean elements, but all mean elements aren't the same. In Chap. 7, we saw that the numerical techniques assume osculating vectors that capture the true time-varying behavior (Fig. 8-1) of the state vector. In contrast, the initial elements for an analytical theory should

---

pg 622 : Clarification

$$M = M_o + n_o \Delta t + \frac{\dot{n}_o}{2}\Delta t^2 + \frac{\ddot{n}_o}{6}\Delta t^3$$

---

pg 623 : Clarification

using these relations. For decades 2-line element sets from Space Command have transmitted the mean-motion rate *already divided by two*, and the acceleration *divided by six*. Don't divide twice!

---

pg 643 : Wording

the formulas for η_{ij} are available. This process is often adequate for general use.

Chapter 9.

pg 652 : Clarification

sile warning assets. It has become increasingly important in determining the location of active and passive objects in space. An important component is the Navy's "fence"—an interferometer that detects all satellites passing through its beams. In 1998, Space Command was tracking more than 9000 objects. Many people believe this number could grow

pg 654 : New Information

Optical Tracking and Identification Facility (MOTIF), Advanced Research Projects Agency (ARPA) - Lincoln C-Band Observables Radar (ALCOR), ARPA Long-Range Tracking and Instrumentation Radar (ALTAIR), and Maui Space Surveillance Station (MSSS).

pg 665 : Clarification

tant to use an accurate method. As an aside, we usually *subtract* the biases from each observation, but you should verify the individual conventions before processing data.

pg 666 : Correction

pg 667 : Correction

$$w_i = \begin{bmatrix} \frac{1}{\sigma_A} & 0 \\ 0 & \frac{1}{\sigma_B} \end{bmatrix} = \begin{bmatrix} w_A & 0 \\ 0 & w_B \end{bmatrix}$$

pg 668 : Clarification

$N - 1$ matters little. We'll adhere to the $N - 1$ convention to ensure commonality with the standard deviation when the mean is zero (see the next paragraph). For Example 9-1, the RMS of the residuals is equal to 0.436 435 ($\sqrt{\frac{1}{7}\sum_{i=1}^{N} y_{o_i} - y_{c_i}} = \sqrt{\frac{1}{7}\sum_{i=1}^{N} y_{o_i} - (0 + 0.667 x_{o_i})}$).

---

pg 681 : Correction

Notice we've assumed the weights are unity values. It's important to note that for equally weighted measurements, this solution simplifies to the linear form of Eq. (9-2), although we still have corrections to the state, rather than the complete state. The $\boldsymbol{A^T A}$ matrix is found by summing the values as shown. For example, the 1,1 component is $(1)^2 + (10.2915)^2 + (40.2476)^2 + (105.9147)^2 = 12{,}944.71$.

---

pg 682 : Correction

---

pg 687 : Correction

$\delta_j = \hat{\boldsymbol{X}}_{nom_j}(0.01)$ modify by 1% of the original value

---

pg 689 : Correction

Fix partials and expand

---

pg 690 : Correction

$$\vec{r}(t) = \vec{r}_o + \vec{v}_o \Delta t + \frac{1}{2}\frac{d\vec{v}}{dt}\bigg|_{t=t_o} \Delta t^2 + \ldots \approx \vec{r}_o + \vec{v}_o \Delta t - \frac{\mu \vec{r}_o}{2r_o^3}\Delta t^2$$

$$\vec{v}(t) = \vec{v}_o + \frac{d\vec{v}}{dt}\bigg|_{t=t_o} \Delta t + \ldots \approx \vec{v}_o - \frac{\mu \vec{r}_o}{2r_o^3}\Delta t$$

$$\left.\frac{\partial \hat{\boldsymbol{X}}}{\partial \hat{\boldsymbol{X}}_o}\right|_{\text{2-body}} = \begin{bmatrix} 1+\frac{3\mu\Delta t^2 r_I^2}{2r_o^5}-\frac{\mu\Delta t^2}{2r_o^3} & \frac{3\mu\Delta t^2 r_I r_J}{2r_o^5} & \frac{3\mu\Delta t^2 r_I r_K}{2r_o^5} & \Delta t & 0 & 0 \\ \frac{3\mu\Delta t^2 r_I r_J}{2r_o^5} & 1+\frac{3\mu\Delta t^2 r_J^2}{2r_o^5}-\frac{\mu\Delta t^2}{2r_o^3} & \frac{3\mu\Delta t^2 r_J r_K}{2r_o^5} & 0 & \Delta t & 0 \\ \frac{3\mu\Delta t^2 r_I r_K}{2r_o^5} & \frac{3\mu\Delta t^2 r_K r_J}{2r_o^5} & 1+\frac{3\mu\Delta t^2 r_K^2}{2r_o^5}-\frac{\mu\Delta t^2}{2r_o^3} & 0 & 0 & \Delta t \\ \frac{3\mu\Delta t r_I^2}{r_o^5}-\frac{\mu\Delta t}{r_o^3} & \frac{3\mu\Delta t r_I r_J}{r_o^5} & \frac{3\mu\Delta t r_I r_K}{r_o^5} & 1 & 0 & 0 \\ \frac{3\mu\Delta t r_I r_J}{r_o^5} & \frac{3\mu\Delta t r_J^2}{r_o^5}-\frac{\mu\Delta t}{r_o^3} & \frac{3\mu\Delta t r_J r_K}{r_o^5} & 0 & 1 & 0 \\ \frac{3\mu\Delta t r_I r_K}{r_o^5} & \frac{3\mu\Delta t r_K r_J}{r_o^5} & \frac{3\mu\Delta t r_K^2}{r_o^5}-\frac{\mu\Delta t}{r_o^3} & 0 & 0 & 1 \end{bmatrix}$$

---

pg 691 : Clarification

We want to obtain $\partial \boldsymbol{X} / \partial \boldsymbol{X}_o$. The equations of motion, $\dot{\hat{\boldsymbol{X}}} = \vec{f}(\vec{r}, \vec{v}, c_D, C_{\ell m}, S_{\ell m})$, depend on the current state (in which the position and velocity vectors depend on the initial state) and the dynamical parameters in the force models. Taking the partial derivatives with respect to the solve-for state vector yields

$$\frac{\partial \dot{\hat{\boldsymbol{X}}}}{\partial \hat{\boldsymbol{X}}_o} = \frac{\partial}{\partial \hat{\boldsymbol{X}}_o}\vec{f}(\vec{r}, \vec{v}, c_D, C_{\ell m}, S_{\ell m}) \tag{9-16}$$

$$\frac{d}{dt}\left[\frac{\partial \hat{\boldsymbol{X}}}{\partial \hat{\boldsymbol{X}}_o}\right] = \frac{\partial}{\partial \hat{\boldsymbol{X}}_o}\left(\frac{d\hat{\boldsymbol{X}}}{dt}\right) = \frac{\partial \vec{f}(\vec{r}, \vec{v}, c_D, C_{\ell m}, S_{\ell m})}{\partial \hat{\boldsymbol{X}}}\frac{\partial \hat{\boldsymbol{X}}}{\partial \hat{\boldsymbol{X}}_o} \tag{9-18}$$

---

pg 692 : Clarification

$$\frac{\partial}{\partial \hat{\boldsymbol{X}}_o}\left(\frac{\partial \hat{\boldsymbol{X}}}{\partial t}\right) = \left\{\frac{\partial \dot{\hat{\boldsymbol{X}}}_{2-body}}{\partial \hat{\boldsymbol{X}}} + \frac{\partial \dot{\hat{\boldsymbol{X}}}_{nonspherical}}{\partial \hat{\boldsymbol{X}}} + \frac{\partial \dot{\hat{\boldsymbol{X}}}_{drag}}{\partial \hat{\boldsymbol{X}}} + \ldots\right\}\frac{\partial \hat{\boldsymbol{X}}}{\partial \hat{\boldsymbol{X}}_o}$$

$$\frac{\partial}{\partial \hat{\boldsymbol{X}}_o}\left(\frac{d\hat{\boldsymbol{X}}}{dt}\right) = \begin{bmatrix} \frac{\partial v_I}{\partial r_I} & \frac{\partial v_I}{\partial r_J} & \frac{\partial v_I}{\partial r_K} & \frac{\partial v_I}{\partial v_I} & \frac{\partial v_I}{\partial v_J} & \frac{\partial v_I}{\partial v_K} \\ \frac{\partial v_J}{\partial r_I} & \cdots & & & & \\ \vdots & & & & & \vdots \\ \frac{\partial a_K}{\partial r_I} & \frac{\partial a_K}{\partial r_J} & \frac{\partial a_K}{\partial r_K} & \frac{\partial a_K}{\partial v_I} & \frac{\partial a_K}{\partial v_J} & \frac{\partial a_K}{\partial v_K} \end{bmatrix} \frac{\partial \hat{\boldsymbol{X}}}{\partial \hat{\boldsymbol{X}}_o}$$

---

pg 693 : Clarification

$$\frac{\partial \hat{\boldsymbol{X}}_{2-body}}{\partial \hat{\boldsymbol{X}}_o} = \begin{bmatrix} 0 & 0 & 0 & 1 & 0 & 0 \\ 0 & 0 & 0 & 0 & 1 & 0 \\ 0 & 0 & 0 & 0 & 0 & 1 \\ -\frac{\mu}{r^3}+\frac{3\mu r_I^2}{r^5} & \frac{3\mu r_I r_J}{r^5} & \frac{3\mu r_I r_K}{r^5} & 0 & 0 & 0 \\ \frac{3\mu r_I r_J}{r^5} & -\frac{\mu}{r^3}+\frac{3\mu r_J^2}{r^5} & \frac{3\mu r_J r_K}{r^5} & 0 & 0 & 0 \\ \frac{3\mu r_I r_K}{r^5} & \frac{3\mu r_J r_K}{r^5} & -\frac{\mu}{r^3}+\frac{3\mu r_K^2}{r^5} & 0 & 0 & 0 \end{bmatrix} \frac{\partial \hat{\boldsymbol{X}}}{\partial \hat{\boldsymbol{X}}_o}$$

$$\frac{\partial \hat{\boldsymbol{X}}_{nonspherical}}{\partial \hat{\boldsymbol{X}}_o} = \begin{bmatrix} 0 & 0 & 0 & 1 & 0 & 0 \\ 0 & 0 & 0 & 0 & 1 & 0 \\ 0 & 0 & 0 & 0 & 0 & 1 \\ \frac{\partial a_I}{\partial r_I} & \frac{\partial a_I}{\partial r_J} & \frac{\partial a_I}{\partial r_K} & 0 & 0 & 0 \\ \frac{\partial a_J}{\partial r_I} & \frac{\partial a_J}{\partial r_J} & \frac{\partial a_J}{\partial r_K} & 0 & 0 & 0 \\ \frac{\partial a_K}{\partial r_I} & \frac{\partial a_K}{\partial r_J} & \frac{\partial a_K}{\partial r_K} & 0 & 0 & 0 \end{bmatrix} \frac{\partial \hat{\boldsymbol{X}}}{\partial \hat{\boldsymbol{X}}_o}$$

---

pg 695 : Correction

pg 700-701 : Correction / Clarification

discuss the final answer to point out important results. If we use Algorithm 58, and remember to subtract the biases from Table 9-3 from each observation, the first ten observations (at the epoch time of JD = 2,449,746.610 150) give us

$$\boldsymbol{A}^{\boldsymbol{T}}\boldsymbol{W}\tilde{\boldsymbol{b}} = \sum_{i=1}^{10} \underset{6\times 3}{\left[\boldsymbol{A}^{\boldsymbol{T}}\right]} \underset{3\times 3}{\left[\boldsymbol{W}\right]} \underset{3\times 1}{\left[\tilde{\boldsymbol{b}}\right]} = \begin{bmatrix} 56{,}960.501 \\ -202{,}775.188 \\ -37{,}935.664 \\ 4{,}321.497 \\ -15{,}652.698 \\ -1{,}311.820 \end{bmatrix}$$

where we've used the weights (noise) from Table 9-3. Be sure to convert the units appropriately.

$$\boldsymbol{W} = \begin{bmatrix} \frac{1}{\sigma_\beta^2} & 0 & 0 \\ 0 & \frac{1}{\sigma_\rho^2} & 0 \\ 0 & 0 & \frac{1}{\sigma_{el}^2} \end{bmatrix} = \begin{bmatrix} \frac{1}{92.5^2} & 0 & 0 \\ 0 & \frac{1}{0.0224^2} & 0 \\ 0 & 0 & \frac{1}{0.0139^2} \end{bmatrix}$$

pg 702 : Clarification

If we look at the standard-deviation values of r_I, for example, we see that our answer has a standard deviation of about 270 m [$(1.797\times10^{-9})^{1/2}$6,378,136.3]. r_I is about 201 m and r_K is about 328 m. Although this answer seems inaccurate, we used only ten observations.

At this point, we haven't considered the coordinate system. Therefore, we've "assumed" a generic inertial frame. If we use these vectors to point a sensor, we must be sure what the system requires—usually true-equator, true-equinox, and so on (see Sec. 1.7). We'll probably have to transform the coordinates.

Notice the similarity between the answers from our simple example and the "complex" answer above. The standard-deviation RMS from the actual experiment (combined cross-track and in-track only) was about 4 m, which coincided with the station bias solved for during the differential correction. If we

pg 708 : Spelling

process because we have a nonlinear system. We *predict* the new state based on previous data, and then *update* that result with the new observations. I'll develop the equations

pg 712 : Wording

Using the linearized dynamics, the resulting updates can be much faster, but a subtlety exists. Don't confuse the nonlinear propagation of the state with the linearized approxima-

tion for the update to the state. When you propagate the state by numerical integration, this is a nonlinear process. When you use Φ to propagate the state update, you've assumed lin

pg 724 : Wording

grator. For the orbit problem, because there are simplified methods to propagate the state to the new time and older computers were slow, a past solution chose *not* to integrate the state but instead used the Φ matrix for two-body motion and let $\delta\boldsymbol{x}$ absorb the dynamics errors, as well as the state corrections based on the observations. This idea should sound

pg 730 : New Information

mismodeling of the orbit. Too little data can also result in our inability to estimate additional state (solve-for) parameters. For instance, Vallado and Carter (1997) show we need more data if we want to solve for biases in addition to the position and velocity vectors. This is especially true for eccentric, deep space, and drag perturbed orbits. We notice the result of too little data as the accuracy of the covariance matrix decreases.

pg 732 : Wording

have enough data to permit a solution to be found. Too little data doesn't permit us to accurately determine the state and bias values.

pg 733 : Wording

Many papers within the literature discuss orbit determination for the TOPEX orbit achieving radial position accuracies around 3 cm. We expect this accuracy for many low-Earth orbits without *significant* drag perturbations in a *post*-processing mode.

pg 736 : Clarification

ods. Error growth depends on force model errors, and on initial errors in the covariance. Be especially cautious in using propagation theories with large process noise characteristics, and the covariance propagation discussed on page 705. Figure 9-14 shows the growth

Chapter 10.

pg 755-56 : Correction / Clarifcation

First, determine initial values to bound the problem. Begin with the horizon-boresight angle:

Therefore, the horizon is $(27.3082)(\pi/180)(R_{\oplus}) = 3039$ km away from the nadir point. It's also useful to find the maximum slant range so you can check later calculations.

Now, determine the range that the sensor can see. Find the ground-range angle by first finding the intermediate angle, γ. Because you're looking directly down ($\eta_{center} = 0°$), use half the complete boresight angle:

You'll always use the smaller value because a satellite can't observe more than a 90° arc of the Earth's surface. Simply subtract or add the ground-range angle to the satellite nadir's location to find the locations of minimum and maximum latitudes:

$$\sin(\gamma) = \frac{r_{sat}\sin(\eta)}{R_{\oplus}} \quad : \text{choose both angles} > 90°, \gamma_{max} = 116.764\,82°, \text{ and } \gamma_{min} = 148.690\,21°$$

Notice that the total ground range is larger than the 340 km (twice 177 km in the $\eta_{center} = 0°$ case) for the observation beneath the satellite. In fact, the 770km groundrange is really an instantaneous value. If the sensor can move ±40°, the actual total ground range is $\Lambda_{FOV} = \Lambda_{max}(2) = 1195$ km. Determine the ground locations the same as before, but because the center of the field-of-view circle is no longer at the nadir point, you must first find the center of the sensor's field-of-view. This involves knowing the direction the sensor is looking. If you assume the satellite is looking perpendicular to the velocity vector, you can locate the center as follows. Because the inclination is 50°, the azimuth for a side-looking sensor is 140°, or 320°. Let's use 140°. Now use Eq. (10-6) to find the center that the sensor is observing. Be sure to find Λ using the process above ($\gamma = 133.6632°$, $\rho = 0.1717$ ER, $\Lambda = 6.3368°$).

$$\sin(\phi_{tgt}) = \cos(\beta)\cos(\phi_{lch})\sin(\Lambda) + \sin(\phi_{lch})\cos(\Lambda)$$

$$\sin(\phi_{tgt}) = \cos(140°)\cos(60°)\sin(6.3368°) + \sin(60°)\cos(6.3368°)$$

$$\phi_{tgt} = 54.9308°$$

From Eq. (10-7),

$$\sin(\Delta\lambda) = \frac{\sin(\beta)\sin(\Lambda)}{\cos(\phi_{lch})} = \frac{\sin(140°)\sin(6.3368°)}{\cos(60°)} \qquad \Delta\lambda = 8.1574°$$

$$\lambda_{tgt} = 48.1574°$$

You can now find the new minimum and maximum latitudes by simply subtracting and adding Λ. Remember that now we use half the distance of the minimum and maximum ramges ($\Lambda = 6.9254 / 2$).

$\phi_{tgtmax} = 58.3935°$, and $\phi_{tgtmin} = 51.4681°$

You can find the locus of points at the edge of the sensor's field of view by repeated use of Eqs. (10-6) and (10-7), letting the azimuth vary from 0° to 360°. For example, at $\beta = 20°$, the center of the FOV is

$\phi_{tgt} = 65.8661°$, and $\lambda_{tgt} = 44.3299°$

---

pg 760 : Correction

$$\Delta\dot{\Omega}_{sec} = \frac{\partial\dot{\Omega}}{\partial i}\Delta i + O(\Delta i)^2$$

---

pg 763 : Correction

$$\Delta i_a = \frac{-A_1}{\dot{\Omega}_{sec}\,\mathrm{TAN}(i)}$$

---

pg 766 : Clarification

$$\Delta\lambda_S = (\omega_\oplus - \dot{\Omega})\Delta\wp_\Omega - \Delta\dot{\Omega}\,\wp_\Omega$$

The final term is really a higher-order effect, thus we will ignore it for this section. The change in $\wp_\Omega$ due to a decaying semimajor axis

$$\Delta\wp_\Omega = \frac{\partial\wp_\Omega}{\partial a}\Delta a + O(\Delta a)^2 \cong \frac{3\pi}{na}\Delta a + O(J_2)$$

---

pg 771 : Correction

orbital plane and positive in the direction of motion, $v = na$), and the expression becomes

$$\Delta v = \frac{n}{2}\Delta a + O(e)$$

---

pg 773 : Correction

$$\Delta v = \frac{n}{2}\Delta a \text{ for small } e$$

---

pg 778 : Correction

$$\Delta\omega_{max} = \sqrt{2\frac{\Delta r_{max}}{ae}\left(\frac{1+e}{1-e}\right)}$$

---

pg 779 : Correction

$$\frac{d\omega}{dt} = \frac{3n}{(1-e^2)^2} J_2 \left(\frac{R_\oplus}{a}\right)^2 \left(1 - \frac{5}{4}\text{SIN}^2(i)\right)\theta$$

$$\theta = 1 + \frac{J_3}{2J_2}\left(\frac{R_\oplus}{a}\right)\left(\frac{1}{(1-e^2)}\right)\left(\frac{\text{SIN}^2(i) - e^2\text{COS}^2(i)}{\text{SIN}(i)}\right)\frac{\text{SIN}(\omega)}{e}$$

equatorial plane or at critical inclination. For these cases, we select ω_o = 90° or 270°, which nulls the eccentricity rate, and we determine the value of e that satisfies $\theta = 0$. For ω_o = 90°, McClain (1987) shows that, if we neglect terms of order $O(e^2)$,

---

pg 787 : Correction

$$\Delta v = \frac{n}{2}\Delta a = \frac{0.956\,443}{2} 0.003\,200 = 0.001\,530 \text{ ER/TU} = 12.0977 \text{ m/s}$$

Remember that you let the satellite drift for twice the drift time, so you'll have to perform a maneuver every 3142 min, and it will be about 12 m/s. This is a large maneuver, and you must correct the orbit

---

pg 801 : Clarification

Visibility checks, which are the only new techniques, divide into several cases. Figure 10-18 shows the geometry. The proximity of the site to the terminator is important when determining how the satellite will appear (visually) from the site. Remember there are several conditions for twilight (Sec. 3.8). The ***terminator*** is the line on the Earth that separates night and day. As Fig. 10-18 shows, there's a period of time after the site passes the terminator when the site is in the dark, but the satellite is illuminated by the Sun. You can see this usually isn't a very long interval, and it depends on the satellite's altitude, but a sunlit satellite is very useful to help acquire satellites if the orbit isn't well-known. Of course as the satellite's altitude increases, the time it's illuminated increases, but the satellite becomes dimmer (its *magnitude* increases) and we'll eventually not be able to see it.

Three conditions are necessary to determine visibility. To establish these conditions, we first find the slant-range vector from the site to the satellite ($\vec{\rho}_{sez} = \vec{r}_{sat_{sez}} - \vec{r}_{siteSEZ}$). This allows us to find the first condition in which the satellite is above or below the horizon. We determine this simply by looking at the third component of the range vector in the *SEZ* coordinate system. It's positive when the satellite is above the horizon. The next condition requires determining if the site is in sunlight or in the Earth's shadow, which we can do by taking the dot product of the Sun and site vectors ($\vec{r}_\odot \cdot \vec{r}_{site}$). If the result is positive, the site is in the Sun; if not, it's in the shadow. We must find the actual angle (ς_{site}) if a twilight condition is used. The final condition consists of determining if the satellite is in the Sun. We must find the angle, ς, from the Sun to the satellite and then the perpendicular distance (*Dist*) from the centerline of the Sun to the satellite [$Dist = r\text{COS}(\varsigma - 90°)$]. I've described this angle in Sec. 3.8, page 194. If the perpendicular distance is larger than

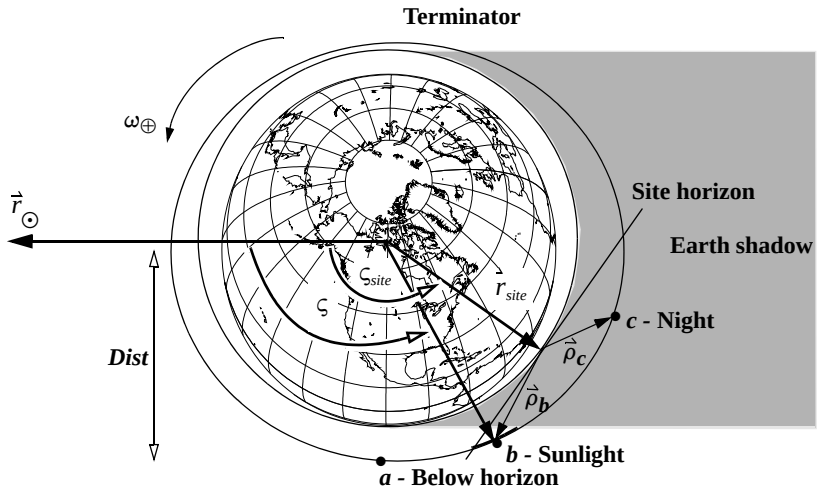

Figure 10-18. Determining Visibility. The visibility of a low-Earth satellite from a ground station, r_{site}, has several cases: the Earth obstructs the view, *a*; the satellite is in the sunlight, *b*; and the satellite is in the Earth's shadow, *c*. We often assume the Earth's shadow is cylindrical. I've shown only one value of ς although there are actually three distinct values of ς corresponding to the three points (*a*, *b*, and *c*).

the Earth's radius, the satellite is in the Sun and is visible to the sensor site. The analysis is more complex if we use the shadow analysis on page 520. By arranging each of the tests in the proper order, we can account for all visibility outcomes. The algorithm shows the proper order. I use three labels for visibility: *Visible* means the satellite is sunlit and the site is in the dark; *radar night* means the satellite isn't sunlit and the site is in the dark; and *radar Sun* means the satellite and site are in the sunlight.

---

pg 802 : Clarification and Correction

Taking these constraints into account, we can write Algorithm 65 to predict look angles for any satellite visible from a ground station. I've shown calculations for azimuth and elevation, but you can also find topocentric right-ascension and declination. The choice of propagator can use any of the techniques discussed in Chap. 7 or Chap. 8. Be careful with the units of the Sun's position vector. The first propagation is included to move the vectors from the satellite epoch to the start time, if they are different.

ALGORITHM 65: PREDICT

$$(\vec{r}_o, \vec{v}_o, JD_o, \vec{r}_{site}, \Delta t, JD_{start}, JD_{end} \Rightarrow JD_i, \rho_i, \beta_i, el_i, \text{Vis}_i)$$

PKEPLER $(\vec{r}_o, \vec{v}_o, JD_{start} - JD_o \Rightarrow \vec{r}, \vec{v})$

LOOP

$JD = JD + \Delta t$

PKEPLER $(\vec{r}, \vec{v}, \Delta t \Rightarrow \vec{r}, \vec{v})$

---

pg 803-804 : Correction

Vis = 'not visible'

UNTIL $JD > JD_{end}$

Note: This problem has changed slightly from the text as the incorrect initial time was used in the original example, thus this example is completly reworked. The answers can be approximated using an epoch of 31 mar 97, 12:50:26.5349846 with some minor adjustments.

Now, as the problem should be.

As an aside, notice that the 2-line elements sets are usually propagated so the satellite is near the equator, thus the small *K*-component. Don't forget to move the satellite to the initial start time. The epoch time is found (UTC = 21:36) giving JD_{epoch} = 2,450,540.400. Now determine an ephemeris for the satellite during the time of interest using the following formulas:

PKEPLER $(\vec{r}_o, \vec{v}_o, JD_{start} - JD_o \Rightarrow \vec{r}, \vec{v})$

LSTIME $(\lambda, JD \Rightarrow \theta_{LST}, \theta_{GST})$

SITE $(\phi_{gd}, h_{ellp}, \theta_{LST} \Rightarrow \vec{r}_{site}, \vec{v}_{site})$ and $\vec{\rho} = \vec{r} - \vec{r}_{site}$

Because we'll get many vectors throughout the time, let's look at the process for one set of vectors on April 2, 1997 at 1:08:0.00 *UTC* (JD = 2,450,540.5472). Determine visibility as follows. The position and velocity vectors are

$$\vec{r} = -2811.3586\hat{I} + 3486.2272\hat{J} + 5069.5546\hat{K} \text{ km}$$

$$\vec{v} = -6.8596\hat{I} - 2.9648\hat{J} - 1.7648\hat{K} \text{ km/s}$$

With θ_{LST} = 136.2944°, the site vector is

$$\vec{r}_{site} = -3411.1225\hat{I} + 3260.3788\hat{J} + 4276.8924\hat{K} \text{ km}$$

Rotating the slant range vector $(\vec{r} - \vec{r}_{site})$ to the *SEZ* coordinate system

$$\vec{\rho} = -773.6886\hat{S} + -577.6745\hat{E} + 326.7046\hat{Z} \text{ km}$$

Because $\vec{\rho}_Z > 0$, we must find coordinates for the Sun to determine the visibility.

SUN $(JD \Rightarrow \vec{r}_\odot)$, $\vec{r}_\odot = 0.9765\hat{I} + 0.1960\hat{J} + 0.0850\hat{K}$ AU

Be sure to convert this vector to ER before finding the dot product, $\vec{r}_\odot \cdot \vec{r}_{site}$. We can find the Sun-satellite angle because the dot product (−8562.835 ER) is less than zero.

$$\text{SIN}(\varsigma) = \frac{|\vec{r}_\odot \times \vec{r}|}{|\vec{r}_\odot||\vec{r}|} \text{ , } \varsigma = 76.0393°$$

The distance quantity is

$$Dist = |\vec{r}| \cos(\varsigma - 90°) = 1.0292 \text{ ER}$$

Because *Dist* is greater than 1.0, the satellite is visible. We can find α, δ, α_t, δ_t, β, *el*, as appropriate. We continue this process for the remaining time interval to arrive at the answers in 4-5. .

TABLE 4-5. Prediction Values for Example 10-6. This table shows sample visibility parameters for three passes in the example problem.

Visibility	**Range km**	β °	***el*** °	***Date***	*UTC* (h/min/s)
Radar Sun	1926.8709	48.9477	3.4758	Apr 1, 97	22:00:0.00
Visible	1738.6880	313.9064	5.6486	Apr 1, 97	23:30:0.00
Visible	1208.9464	341.3249	14.0546	Apr 1, 97	23:32:0.00
Visible	1151.0123	26.7924	15.3278	Apr 1, 97	23:34:0.00
Visible	1617.3545	58.3564	7.2074	Apr 1, 97	23:36:0.00
Visible	1787.4217	310.1824	5.0535	Apr 2, 97	01:06:0.00
Visible	1019.3320	323.2531	18.6937	Apr 2, 97	01:08:0.00
Radar Night	574.8788	29.2134	41.6979	Apr 2, 97	01:10:0.00
Radar Night	1040.3959	92.3719	18.1174	Apr 2, 97	01:12:0.00
Radar Night	1811.9563	104.9278	4.7792	Apr 2, 97	01:14:0.00

Appendix A

pg 836 : Wording

for

Appendix C

pg 846-852 : Clarification

B.1.3 Evaluating Density

Jacchia used a standard exponential relation to evlauate density. From Eq. (7-31),

$$\rho_{std} = \rho_o \mathrm{EXP}\left[-\frac{h_{ellp} - h_o}{H}\right] \tag{B-10}$$

For altitudes below 200 km, we include the *geomagnetic effect* on density:

We then apply the correction terms of Eq. (B-7), Eq. (B-8), and Eq. (B-9) to the standard density:

$$(\Delta \log_{10}\rho)_{corr} = (\Delta \log_{10}\rho)_G + (\Delta \log_{10}\rho)_{SA} + (\Delta \log_{10}\rho)_{LT}$$

giving the final corrected density

$$\rho(h_{ellp}) = \rho_{std}(h_{ellp})\ 10^{(\Delta \log_{10}\rho)_{corr}} \tag{B-11}$$

of density from 0 to 90 km are important mainly for calculating reentry and are usually handled by standard atmospheres (See Sec. 7.6.2). The end result is that we use Eq. (B-11), Eq. (B-12), or Eq. (B-12) for the standard density in Eq. (B-11).

We don't consider hydrogen significant in determining density below 125 km, thus thus the summation from i = 1 to 5 in Eq. (B-12). We could evaluate the density at 100 km [ρ(100)] by Eq. (B-11), but this approach is intensive as we saw in the last section! Long et achieve the individual effect of the *five* basic atmospheric constituents (Table B-3) on the standard density. We include $\rho_6(h_{ellp})$ for altitudes over 500 km.

$$\rho_{std_{125}}(h_{ellp}) = \sum_{i=1}^{5} \rho_i(125)\left(\frac{T_x}{T(h_{ellp})}\right)^{1+a_i+\gamma_i}\left(\frac{T_{corr}-T_x}{T_{corr}-T_o}\right)^{\gamma_i} + \rho_6(h_{ellp})$$
$$\gamma_i = \frac{M_i g_o R_{pole}^2}{R_\ell^\prime T_{corr}}\left(\frac{T_{corr}-T_x}{T_x-T_o}\right)\left(\frac{35}{6481.766}\right) \quad \text{(B-12)}$$

Although we can explicitly determine the constituent densities, ρ_i (125) from Eq. (B-12), Draper Laboratory uses a polynomial curve fit approximation in the Goddard Trajectory Determination System (Long et al., 1989, 4-49).

$$\rho_i(125) = M_i 10^{\sum_{j=0}^{6} \delta_{ij} T_{corr}^j}$$

Here, δ_{ij} are curve-fit coefficients in Table B-4, and M_i are from Table B-3

---

pg 856 : Clarification

A ***scalar matrix*** is sometimes used in astrodynamics. It's a matrix with all the diagonal terms equal to some constant, and all other terms equal to zero.

---

pg 869 : Clarification

To alleviate the problems in modeling Fourier series and polynomial wiggle we use cubic and quintic spline functions. ***Polynomial wiggle*** is a phenomena where large variations occur between data points due to the extrema of the polynomial (Matthews, 1987, 231). For instance, a fifth-order polynomial may fit each data point, while simultaneously diverging large amounts between data points. In this case, a second-order polynomial is probably a better answer. Curve fitting by ***cubic splining*** uses function values and their time derivatives at the beginning and end of a time interval to create a third-order polynomial.

Appendix D

---

pg 875 : Clarification

$$\boldsymbol{C_t = -J_t}$$

---

pg 880-881 : Correction

1992 for date

pg 884-886 : Correction

Reference Mean Equinox of <u>Date in Degrees</u>

Remember that the semimajor axis and eccentricity will be identical to the degree expressions already shown.

Mercury

$$i = 7.004\,986 + 0.001\,821\,5T_{UT1} - 0.000\,018\,09T_{UT1}^2 + 0.000\,000\,053T_{UT1}^3$$

$$\Omega = 48.330\,893 + 1.186\,189\,0T_{UT1} + 0.000\,175\,87T_{UT1}^2 + 0.000\,000\,211T_{UT1}^3$$

$$\tilde{\omega} = 77.456\,119 + 1.556\,477\,5T_{UT1} + 0.000\,295\,89T_{UT1}^2 + 0.000\,000\,056T_{UT1}^3$$

$$\lambda_M = 252.250\,906 + 149{,}474.072\,2491T_{UT1} + 0.000\,30397T_{UT1}^2 + 0.000\,000\,018T_{UT1}^3$$

Venus

$$i = 3.394\,662 + 0.001\,003\,7T_{UT1} - 0.000\,000\,88T_{UT1}^2 - 0.000\,000\,007T_{UT1}^3$$

$$\Omega = 76.679\,920 + 0.901\,119\,0T_{UT1} + 0.000\,406\,65T_{UT1}^2 - 0.000\,000\,080T_{UT1}^3$$

$$\tilde{\omega} = 131.563\,707 + 1.402\,218\,8T_{UT1} - 0.001\,073\,37T_{UT1}^2 - 0.000\,005\,315T_{UT1}^3$$

$$\lambda_M = 181.979\,801 + 58519.213\,030\,2T_{UT1} + 0.000\,310\,60T_{UT1}^2 + 0.000\,000\,015T_{UT1}^3$$

Earth

$$i = 0.0$$

$$\Omega = 0.0$$

$$\tilde{\omega} = 102.937\,348 + 1.719\,526\,9T_{UT1} + 0.000\,459\,62T_{UT1}^2 + 0.000\,000\,499T_{UT1}^3$$

$$\lambda_M = 100.466\,449 + 36000/769\,823\,1T_{UT1} + 0.000\,303\,68T_{UT1}^2 + 0.000\,000\,021T_{UT1}^3$$

Mars

$$i = 1.849\,726 - 0.000\,601\,0T_{UT1} + 0.000\,012\,76T_{UT1}^2 - 0.000\,000\,006T_{UT1}^3$$

$$\Omega = 49.558\,093 + 0.772\,092\,3T_{UT1} + 0.000\,016\,05T_{UT1}^2 + 0.000\,002\,325T_{UT1}^3$$

$$\tilde{\omega} = 336.060\,234 + 1.841\,033\,1T_{UT1} + 0.000\,135\,15T_{UT1}^2 + 0.000\,000\,318T_{UT1}^3$$

$$\lambda_M = 355.433\,275 + 19141.696\,474\,6T_{UT1} + 0.000\,310\,97T_{UT1}^2 + 0.000\,000\,015T_{UT1}^3$$

Jupiter

i $= 1.303\,270 - 0.005\,496\,6T_{UT1} + 0.000\,004\,65T_{UT1}^2 - 0.000\,000\,004T_{UT1}^3$

Ω $= 100.464\,441 + 1.020\,955\,0T_{UT1} + 0.000\,401\,17T_{UT1}^2 + 0.000\,000\,569T_{UT1}^3$

$\tilde{\omega}$ $= 14.331\,309 + 1.612\,666\,8T_{UT1} + 0.001\,031\,27T_{UT1}^2 - 0.000\,004\,569T_{UT1}^3$

λ_M $= 34.351\,484 + 3036.302\,788\,9T_{UT1} + 0.000\,223\,74T_{UT1}^2 + 0.000\,000\,025T_{UT1}^3$

Saturn

i $= 2.488\,878 - 0.003\,7363T_{UT1} - 0.000\,015\,16T_{UT1}^2 + 0.000\,000\,089T_{UT1}^3$

Ω $= 113.665\,524 + 0.877\,097\,9T_{UT1} - 0.000\,120\,67T_{UT1}^2 - 0.000\,002\,380T_{UT1}^3$

$\tilde{\omega}$ $= 93.056\,787 + 1.963\,769\,4T_{UT1} + 0.000\,837\,57T_{UT1}^2 + 0.000\,004\,899T_{UT1}^3$

λ_M $= 50.077\,471 + 1223.511\,014\,1T_{UT1} + 0.000\,519\,52T_{UT1}^2 - 0.000\,000\,003T_{UT1}^3$

Uranus

i $= 0.773\,196 + 0.000\,774\,4T_{UT1} + 0.000\,037\,49T_{UT1}^2 - 0.000\,000\,092T_{UT1}^3$

Ω $= 74.005\,947 + 0.521\,125\,8T_{UT1} + 0.001\,339\,82T_{UT1}^2 + 0.000\,018\,516T_{UT1}^3$

$\tilde{\omega}$ $= 173.005\,159 + 1.486\,378\,4T_{UT1} + 0.000\,214\,50T_{UT1}^2 + 0.000\,000\,433T_{UT1}^3$

λ_M $= 314.055\,005 + 429.864\,056\,1T_{UT1} + 0.000\,304\,34T_{UT1}^2 + 0.000\,000\,026T_{UT1}^3$

Neptune

i $= 1.769\,952 - 0.009\,308\,2T_{UT1} - 0.000\,007\,08T_{UT1}^2 + 0.000\,000\,028T_{UT1}^3$

Ω $= 131.784\,057 + 1.102\,205\,7T_{UT1} + 0.000\,260\,06T_{UT1}^2 - 0.000\,000\,636T_{UT1}^3$

$\tilde{\omega}$ $= 48.123\,691 + 1.426\,2677T_{UT1} + 0.000\,379\,18T_{UT1}^2 - 0.000\,000\,003T_{UT1}^3$

λ_M $= 304.348\,665 + 219.883\,309\,2T_{UT1} + 0.000\,309\,26T_{UT1}^2 + 0.000\,000\,018T_{UT1}^3$

Pluto

i $= 17.132\,33°$

Ω $= 110.406\,5°$

$\tilde{\omega}$ $= 224.6148°$

λ_M $= 218.887\,35°$

Back Cover

pg back cover : Clarification

This table lists some common Julian dates for selected years. Remember that the JD is at 12 h *UT*. The table also gives the Greenwich Sidereal Time for January 1 at 0 h *UT* for each year. The years 1900, 1950, and 2000 are common for use in coordinate systems.